

Boston University

OpenBU

<http://open.bu.edu>

Theses & Dissertations

Boston University Theses & Dissertations

2015

Topology control algorithms in power systems

<https://hdl.handle.net/2144/16306>

Boston University

BOSTON UNIVERSITY
COLLEGE OF ENGINEERING

Dissertation

TOPOLOGY CONTROL ALGORITHMS IN POWER SYSTEMS

by

EVGENIY GOLDIS

B.S., Harvey Mudd College, 2004
M.A., Boston University, 2007

Submitted in partial fulfillment of the
requirements for the degree of
Doctor of Philosophy

2015

© 2015 by
EVGENIY GOLDIS
All rights reserved

Approved by

First Reader

Michael Caramanis, Ph.D.
Professor of Mechanical Engineering
Professor of Systems Engineering

Second Reader

Ioannis Ch. Paschalidis, Ph.D.
Professor of Electrical and Computer Engineering
Professor of Systems Engineering
Professor of Biomedical Engineering

Third Reader

Pablo A. Ruiz, Ph.D.
Research Associate Professor of Mechanical Engineering

Fourth Reader

Alex Stanković, Ph.D.
Alvin H. Howell Professor in Electrical Engineering
Tufts University

Acknowledgments

I would like to acknowledge the support from PJM in providing market data and for general advice and feedback in our modeling efforts. Additionally, I would like to acknowledge AIMMS and Polaris for providing the software tools that were instrumental to the progress of this work and especially Polaris for making numerous changes to the PSO tool to support the modeling efforts. Finally, the work presented herein was funded in part by the Advanced Research Projects Agency-Energy (ARPA-E), U.S. Department of Energy, under Award Number DE-AR0000223

TOPOLOGY CONTROL ALGORITHMS IN POWER SYSTEMS

EVGENIY GOLDIS

Boston University, College of Engineering, 2015

Major Professor: Michael Caramanis, Ph.D., Professor of Mechanical Engineering,
Professor of Systems Engineering

ABSTRACT

This research focuses on improving the efficiency of power market operations by providing system operators additional tools for managing the costs of supplying and delivering electricity. A transmission topology control (TC) framework for production cost reduction based on a shift factor (SF) representation of branch and breaker flows is proposed. The framework models topology changes endogenously while maintaining linearity in the overall Mixed Integer Linear Programming (MILP) formulation. This work develops the DC lossless, and loss-adjusted TC formulations that can be used in a Day-Ahead or intra-day market framework as well as an AC-based model that can be used in operational settings. Practical implementation choices for the Shift Factor formulation are discussed as well as the locational marginal prices (LMPs) under the TC MIP setting and their relation to LMPs without TC. Compared to the standard $B\theta$ alternative used so far in TC research, the shift factor framework has significant computational complexity advantages, particularly when a tractably small switchable set is optimized under a representative set of contingency constraints. These claims are supported and elaborated by numerical results.

Contents

1	Introduction	1
2	The Optimal Power Flow Problem	6
2.1	Notation and Definitions	6
2.2	AC Optimal Power Flow	7
2.3	$B\theta$ Linearization	9
2.4	Shift Factor Formulation	12
2.5	Shift Factor Formulation With Breakers	15
2.6	LMPs in the Shift Factor OPF	19
3	Topology Control - Branch Switching	21
3.1	$B\theta$ Topology Control Formulation	21
3.2	Shift Factor Topology Control Formulation	23
3.2.1	Flow-Cancelling Transactions	25
3.2.2	FCT MIP Formulation of Topology Control	27
3.2.3	LMPs under the FCT MIP	29
3.2.4	Formulation Implementation Aspects	31
3.3	Numerical Experience on a Large System	33
3.4	TC Formulation with Loss Adjusted Shift Factors	37
3.5	TC MIP Formulation with Losses	40
3.5.1	LMPs and Loss-Adjusted Formulation	43
3.5.2	Loss-Adjusted TC Simulations on the IEEE 118-bus System	45
3.6	TC Formulation with AC Modeling	47

3.6.1	AC Modeling Results for the PJM System	50
4	Substation Reconfiguration	56
4.1	MIP Formulation with BCTs	57
4.1.1	MIP Formulation with BCTs and FCTs	60
4.2	Breaker Opening Incremental Flows	61
4.3	BOIF Formulation	65
4.3.1	Joint BOIF and Branch Switching Formulation	70
4.4	Breaker Modeling	71
4.4.1	BOIF and BCT Applications	73
4.4.2	Substation Test System	74
4.4.3	Simulation Results	76
5	Concluding Remarks	82
	Bibliography	84
	Curriculum Vitae	87

List of Tables

3.1	LP Formulation Results	35
3.2	Constraint and Variable Statistics – LP Case with Contingencies	35
3.3	MIP Formulation Results	36
3.4	Median Number of Line Openings and Average Per-unit Congestion Costs Savings with different loss modeling assumptions over 100 Samples	45
3.5	Summary of Savings achieved by TCA (millions of dollars)	50
3.6	Summary of Line Switchings by Voltage Level	54
3.7	Topology Change Statistics Summary - Summer Week	54
4.1	BOIF and BCT Solve Times (seconds)	78
4.2	Topology Control Actions in the BCT, BOIF, FCT and Joint BOIF+FCT formulations	80

List of Figures

3.1	Opening line k (top) is equivalent from the point of view of the rest of the system as inserting a flow-cancelling transaction at virtual buses m' and n' , infinitely close to m and n , respectively, and along line k (bottom).	26
3.2	Number of Lines Opened in DC MIP Formulations	46
3.3	Algorithm Structure	49
3.4	Cost of Congestion	51
3.5	Savings	51
3.6	% Savings Captured	52
3.7	Branches Open with TCA - 2010 Summer	52
3.8	Branches Open with TCA - 2010 Winter	52
3.9	Branches Open with TCA - 2010 Shoulder	53
4.1	(a) shows part of a network with a breaker z and an FCT v across branch k that we assume is necessary to emulate the opening of breaker z . The resulting flows on the 3 branches are labelled. (b) shows the network with the breaker physically opened and the resulting flows on the 3 branches . . .	62
4.2	small 6-bus network with branches labeled as ℓ_1 through ℓ_8 and busses b_1 through b_6	66
4.3	Stylized ring bus configuration.	68
4.4	Breakers kept open in the breaker closing transaction (BCT) formulation and breakers opened in the breaker opening incremental flow (BOIF) formulation. 76	
4.5	Number of breakers operated in the BCT and BOIF models	77
4.6	Solve times, reported in seconds, for the BCT and BOIF formulations . . .	78

4.7	Branch and breaker openings under the BOIF, FCT and joint formulations	79
4.8	Cost of Congestion Savings (%) for the BOIF, FCT and joint formulations	80

List of Symbols

Vectors are indicated by lower case bold, matrices by upper case bold, and scalars by lower case italic characters indexed appropriately. Upper limits are indicated by an over-bar, and lower limits by an under-bar. Sensitivities are indicated with Greek characters.

m, n Nodes.

k, ℓ Branches.

m_ℓ Branch ℓ from node.

n_ℓ Branch ℓ to node.

τ Contingent topologies.

z Zero-impedance breakers.

r Substation *cutset* that separates a busbar from the rest of the substation.

Contingent Topology-Dependent Parameters and Variables

For contingent topology τ ,

\mathbf{A}_τ Reduced incidence matrix.

\mathbf{B}_τ Reduced nodal susceptance matrix.

$\mathbf{f}_\tau^{\mathcal{N}}$ Vector of real power flows on branches.

$\mathbf{f}_\tau^{\mathcal{Z}}$ Vector of real power flows on zero-impedance breakers.

\mathbf{g}_τ^0 Bias from linearization of transmission flows.

$\underline{\mathbf{f}}_\tau, \bar{\mathbf{f}}_\tau$ Vectors of transmission limits.

$\mathbf{v}_\tau^{\mathcal{Z}}$ Vector of breaker closing transactions.

$\mathbf{v}_\tau^{\mathcal{S}}$ Vector of flow-cancelling transactions.

δ_τ Vector of breaker opening incremental flows (BOIFs).

Ψ_τ Shift factor matrix.

- $\hat{\Psi}_\tau$ Shift factor matrix with candidate breakers removed.
- $\Psi_\tau^{\mathcal{M}}$ Shift factor matrix associated with monitored branches.
- $\Psi_\tau^{\mathcal{Z}}$ Shift factor matrix associated with zero-impedance breakers.
- $\Phi_\tau^{\mathcal{MZ}}$ PTDF matrix of monitored branches for transfer through zero-impedance breakers.
- $\hat{\Phi}_\tau$ PTDF matrix with candidate zero-impedance breakers removed.
- Γ_τ Matrix of PTDF ratios for zero-impedance breakers.
- $\gamma_\tau^{\mathcal{Z}}$ vector corresponding to a single zero-impedance breaker in Γ_τ
- $\psi_{\ell\tau}^m$ Element of Ψ for branch ℓ , node m .
- $\phi_{\ell\tau}^k$ PTDF of branch ℓ for a transfer across branch k .
- λ Power balance shadow price.
- $\underline{\mu}_\tau$ Shadow price of lower flow limit for monitored branch constraints.
- $\overline{\mu}_\tau$ Shadow price of upper flow limit for monitored branch constraints.
- $\underline{\alpha}_\tau$ Shadow prices of lower flow limit for switchable branch constraints.
- $\overline{\alpha}_\tau$ Shadow prices of upper flow limit for switchable branch constraints.
- $\phi_{\ell\tau}^k$ LODF of branch ℓ for the outage of branch k .
- Contingent Topology-Independent Parameters and Variables*
- $\mathbf{1}$ Vector of ones.
- \mathbf{I} Identity matrix.
- $\tilde{\mathbf{B}}$ Branch susceptance matrix for branches (non zero-impedance).
- $\mathbf{t}^{\mathcal{S}}$ Vector with the 0/1 state of branches
- $\mathbf{t}^{\mathcal{Z}}$ Vector with the 0/1 state of zero-impedance breakers
- \mathbf{c} Vector of nodal generation variable cost.
- \mathbf{p}, \mathbf{l} Vector of nodal generation and loads.
- τ_0 Full topology without contingencies.
- $\Psi^{\mathcal{Z}}$ Matrix of all $\Psi_\tau^{\mathcal{Z}}$.
- $\Psi^{\mathcal{M}}$ Matrix of all $\Psi_\tau^{\mathcal{M}}$.
- M Sufficiently large number.

Chapter 1

Introduction

In modern power markets, an Independent System Operator (ISO), schedules generating resources to ensure that at every moment in time generation equals electricity consumption. This scheduling process generally takes place through two stages. In the first stage the ISO solves a Unit Commitment (UC) model to “commit” generating capacity, that is, determine which power plants need to be on-line and ready to operate on the next day. In part, this first stage is necessary to account for inflexibilities in the market. Many power plants, for example, have technological and economic requirements for the amount of time they need to be running before they can be shutdown, the amount of time they should be off-line before being started and the amount of time needed for them to start. Due to such constraints, the ISO needs to plan ahead to ensure there is enough generating capacity on-line to serve demand and to account for possible contingency events (a power plant fails to start due to mechanical failure, for example). In the second stage the ISO solves the Economic Dispatch (ED) model and sends dispatch signals to power plants with instructions for how much to generate. The second stage accounts for changes in available information and contingency events. When solving the UC model, for example, the system operator only has a forecast of electricity demand. This forecast will become more and more accurate as it gets closer to “real time” and hence, the output of individual power plants will change from the UC to the ED model solution. Similarly to the demand forecast, wind and solar forecasts are inherently inaccurate and will impact the amount of generation from renewable resources, something the ISO needs to account for in the ED model.

In solving the UC model, the ISO’s goal is to minimize total generation costs. In very

general terms, the ISO collects price/quantity bids from all power plant owners and using the demand forecast, determine which power plants should be kept on-line, brought on-line or taken off-line for each hour of the next day. In reality there are many constraints that need to be satisfied in this process that make the problem very difficult. As mentioned above, every power plant has its own economic and technological constraints that must be satisfied, and the decision for which power plants to turn on and off are binary, placing this problem in the Mixed Integer Programming domain. In addition, there are many transmission network constraints that the ISO must satisfy, discussed in greater detail in the next chapter.

The traditional ED model is a simpler one to solve. The ISO's objective is still the minimization of cost but the state (on-line or not) of all generators has already been determined in the UC model. The main decisions in the ED model are the output levels of each power plant, which under some assumptions described in Chapter 2, simplify the model formulation and place it in the Linear Programming domain.

The operation of the power market described here is meant to give the reader a high level understanding and to provide a general structure for framing the rest of this work. Up to now we have described the power market in terms of models but the power market, as the name suggests is made up of markets. The Day-Ahead (DA) market is typically associated with the UC model while the Real-Time market is associated with the ED model (although some form of the UC and ED models are solved in multiple markets). In addition to solving these models there are many financial transactions and administrative process that take place. The rest of this work will mainly focus on the ED model and specifically on the state of the transmission network. To state it more formally, the ED model determines the generation of every power plant by minimizing generation cost subject to generator and transmission (power flow) constraints. Power flows distribute over an AC network following Kirchhoff's laws. As such, flows depend on the load profile, generation dispatch and transmission topology, including transmission system characteristics, settings and connectivity status. While the ISO determines the on/off state of power plants in

the UC model, the open/closed state of branches and breakers is typically considered to be fixed or non-controllable in both UC and ED. Transmission topology changes are considered as inputs to the decision processes, such as a list of pre-specified contingencies, or as a transmission maintenance schedule, and not as a decision variable.¹

The lack of topology control (TC) application persists in spite of substantial research in the area over the last decades. Corrective control [2–4], security enhancements [5,6] and loss minimization [7,8] are some examples of past investigations. More recently, topology control has been examined for its potential cost reduction in economic dispatch [9–11] and unit commitment [12]. Production cost saving opportunities enabled through congestion mitigation by topology control are very promising. Reasonable projections of quantitative results obtained for large systems suggesting several billion dollars in annual savings in the U.S. alone. In this work, the objective of TC is production cost minimization.

This work focuses on two forms of topology control. The first is branch switching, the opening/closing of transmission branches. The second is substation reconfiguration, the opening/closing of zero-impedance breakers within a substation. In both cases, the algorithms developed aim to extract more value out of transmission facilities by:

- Providing additional operational controls to help manage congestion and to respond to contingency situations
- Significantly reducing generation costs
- Enabling higher levels of variable renewable penetration
- Increasing system reliability

To put this problem into perspective, transmission congestion costs in the Pennsylvania-JerseyMaryland (PJM), the largest ISO, alone totaled more than 1.5 billion in 2010, and U.S. costs are estimated at 510 billion per year.

¹Exceptions exist, however. Rule-based decisions like *operating guides* and *special protection schemes* open or close pre-specified breakers upon the occurrence of contingencies or other pre-specified phenomena [1]

Congestion costs result from out-of-merit-order dispatch, i.e., when transmission limits force more expensive generation to be dispatched before fully utilizing less expensive resources. Congestion on a transmission branch along one path between two nodes can limit the total transfer capability between those nodes, even if excess transmission capacity exists on a different path between them. This results because power flows are determined by Kirchhoff's Laws and are typically not routable. However, branches that limit transfer capability, as well as branches that feed or are fed by these limiting branches, are potentially desirable to open. Opening such branches effectively increases the impedance of paths containing these limiting facilities, reducing the flow through them, increasing it on the non-limiting facilities and thus increasing total transfer capability. Transmission topology control (TC), i.e., appropriate changes of transmission line status, can therefore redistribute power flow and lower congestion costs. Historically, due to generation controllability, load predictability, and the vertically integrated utility structure, there has been limited power-transfer variability. However, with industry restructuring and the impending large-scale integration of renewable generation and flexible demand, this variation is significantly increasing. For example, the Electric Reliability Council of Texas (ERCOT) has been forced to change operating rules as a result of increased wind capacity in the coastal region and its impacts on transmission congestion. Consider an area with high penetration of wind and solar plants. These generation sources usually are not collocated and generate during different times of the day, varying their profile from day to day. In addition, the location of loads changes as people go to work in the morning and return home in the early evening. As such, optimal topology control is a dynamic optimization problem as the locations between which it is optimal to increase the transfer capability change many times throughout the day.

The algorithms we develop must work on large (13,000+) bus systems and satisfy all existing reliability constraints (connectivity, security, transient and voltage stability). For these algorithms to be included into the existing economic dispatch process, they must also meet computation effort requirements set by the ISO (5 minutes for the ED problem,

for example). Excessive computational times have been a key barrier to systematic use of TC for production cost minimization. The main cause for these excessive times has been the formulation choice for solving the ED problem. In current literature, there are two common formulations for the ED problem. The first is called the $B\theta$ model and expresses the power flows on a branch explicitly as a function of the angle differences between the branch terminals. The second is called the shift factor formulation and uses sensitivities (derivatives) to model transmission flows as a function of injections and withdrawals at buses in the network (a full derivation of both formulations is discussed in Chapter 2). In previous work, the TC problem has been formulated as a mixed integer linear program (MILP) using the $B\theta$ representation of power flows under DC assumptions. While this representation is a very natural extension of the standard $B\theta$ model it imposes an extremely large number of variables and constraints.

This work contributes to the power systems field in four main areas. First, it extends the lossless shift factor economic dispatch model to incorporate topology control while maintaining linearity in the underlying formulation. Second, it derives modified shift factors that allow losses to be incorporated and shows that topology control can be beneficial even in the absence of congestion. Third, this work formulates two novel formulations for modeling substation reconfiguration and proves that zero-impedance breakers can be precisely represented within the shift factor ED model. Finally, through simulations using actual data from the PJM System Operator, this work demonstrates that topology control can already be incorporated with other tools used in the control room and has potential to provide significant benefits.

Chapter 2

The Optimal Power Flow Problem

2.1 Notation and Definitions

For the purpose of this work, a transmission network is defined by a set of substations, busbars, busses (or nodes), branches and breakers. A bus is an electrical device that connects two or more transmission branches. A substation is another type of electrical device that performs a variety of functions, but for our purposes a substation is an abstract object comprised of two or more busbars connected by zero-impedance breakers. In power flow modeling the connection between busbars within a substation is typically represented as one of zero-impedance and when we discuss topology control in the context of substation reconfiguration we will be referring to the opening and closing of zero-impedance breakers. When a set of busbars within a substation are connected via breakers, these busbars effectively act as a single electrical device and in this work we will collapse such busbars into their equivalent bus (unless the breakers between them are being considered for topology control). A transmission branch will refer to a non zero-impedance facility connecting two busses, such as a line or transformer.

The connectivity of the network is represented using a reduced $L \times N - 1$ incidence matrix, \mathbf{A} where L is the number of branches and breakers and N is the number of nodes. Each row ℓ has elements -1 and 1 in the columns corresponding to the *from* and *to* nodes of line ℓ respectively, and 0 for all other nodes. The matrix is called reduced because one column, corresponding to what is called the reference bus, is excluded from \mathbf{A} . This is a standard approach in many graph theory applications and it easy to see that with $N - 1$

columns all connectivity information is maintained (including all columns would lead to a matrix that is not of full rank). For convenience we will call bus N the reference bus.

At any point in time, a subset of the transmission branches may be disconnected due to contingencies, planned actions such as maintenance or due to topology control decisions. The resulting topology τ represents a change to the state of the transmission network and is characterized by a change to the incidence matrix, denoted by \mathbf{A}_τ . In the rest of this work a change in topology will be used to represent contingency constraints. Contingency constraints enforce the flow on one branch in the event that another branch is taken out of service. For example, in the case of two parallel lines, the system operator may allow more power to flow through one of the branches when the other one is taken out of service. While both the incidence matrix and flow limits may change with τ , we assume that generation and load are independent of the topology (though they need not be, e.g., under corrective control).

2.2 AC Optimal Power Flow

The Optimal Power Flow (OPF) problem is at the heart of the unit commitment and economic dispatch models. The OPF objective is the minimization of generation cost subject to transmission constraints. In this section we formulate the AC version of the OPF problem and discuss its application to the UC and ED models. For simplicity we only consider real power flows and ignore reactive power. This assumption is consistent with market models used for UC and ED. We will briefly discuss reactive power in chapter 3 but the majority of this work focuses on DC based modeling so we ignore reactive power for the rest of this chapter. We define a state vector for all nodes as

$$\mathbf{s} = \begin{bmatrix} \theta \\ \mathbf{V} \end{bmatrix} \quad (2.1)$$

Using this state variable we can express the formulation as follows

$$\min_{p, \theta, V} C(p) \quad (2.2)$$

$$\text{s.t.} \quad (2.3)$$

$$W(\mathbf{s}, \mathbf{p}) = \mathbf{0} \quad (2.4)$$

$$\underline{\mathbf{f}} \leq \mathbf{f} \leq \bar{\mathbf{f}} \quad (2.5)$$

$$\underline{\mathbf{p}} \leq \mathbf{p} \leq \bar{\mathbf{p}} \quad (2.6)$$

Where $C(\mathbf{p})$ is a typically piece-wise linear cost function of generation, \mathbf{p} . Vectors $\underline{\mathbf{f}}, \bar{\mathbf{f}}$ are lower and upper branch limits and $\underline{\mathbf{p}}, \bar{\mathbf{p}}$ are lower and upper generation limits. Equation (2.4) represents the nodal energy balance constraint that is common to most optimization problems involving networks. Equation (2.5) states that the flow on transmission lines should be within the upper and lower bounds and equation (2.6) states the same thing for generation levels. Since flows on transmission branches follow Kirchhoffs laws, for a particular node n and line ℓ going from node i to node j we can express equations (2.4) and (2.5) as

$$W^n(\mathbf{s}, \mathbf{p}) = (V^n)^2 g_{nn} + \sum_{\substack{m=1 \\ m \neq n}}^N (V^m [g_{nm} \cos(\theta^n - \theta^m) - b_{nm} \sin(\theta^n - \theta^m)]) - (p^n - l^n) \quad (2.7)$$

$$f_\ell = h_\ell(s) = g_\ell \left[(V^i)^2 - (V^i V^j) \cos(\theta^i - \theta^j) \right] + \tilde{b}_\ell V^i V^j \sin(\theta^i - \theta^j) \quad (2.8)$$

Where g_{nm} and b_{nm} represent the conductance and susceptance between nodes n and m respectively. For convenience and without loss of generality we assume that nodal load \mathbf{l} is fixed and only the generation is controllable. The elements b_{nm} form a nodal susceptance matrix \mathbf{B} defined as follows

$$\mathbf{B} = \mathbf{A}' \tilde{\mathbf{B}} \mathbf{A} \quad (2.9)$$

with individual elements having the structure below

$$b_{ii} = \sum_{\ell \in i} \tilde{b}_{\ell} \quad (2.10)$$

$$b_{ij} = \mathbf{1}_{\ell=(i,j)}(-\tilde{b}_{\ell}) \quad (2.11)$$

The indicator function $\mathbf{1}_{\ell=(i,j)}$ is 1 when branch ℓ connects nodes i and j ¹. The formulation defined by constraints (2.2)-(2.6) defines a simplified AC OPF for real power. Despite this simplification, the model is non-convex. For a system such as PJM that has 13,000+ busses and 20,000+ branches, solving such a problem becomes difficult. In the UC model, the OPF additionally includes the binary decision variables that determine which generators to turn on and off. Attempting to solve the AC-based unit commitment model requires solving a non-convex, mixed integer programming problem. Even with the current state of the art solvers, such a problem is impractical given the ISO's time constraints. To get around this complexity, system operators solve a linearized version of the AC OPF. The linearized version is called the DC OPF and in the next two sections we present the two common linearizations: $B\theta$ and Shift Factor. In actual operations, system operators solve linearized versions of the AC OPF and then verify the solution against the full set of AC power flow constraints in an iterative fashion. This approach guarantees that the result of the DC OPF is reliable while maintaining fast solution times.

2.3 $B\theta$ Linearization

In this section we derive the $B\theta$ OPF formulation with only non zero-impedance branches (we expand the formulation to include breakers in section 2.5). The $B\theta$ formulation relies on the following three assumptions

- $V^n \approx 1 \quad \forall n$
- $\theta^i - \theta^j \approx 0 \quad \forall \ell = (i, j)$

¹The nodal conductance matrix has a similar structure

- $r_\ell \ll x_\ell$

The first two assumptions state that voltages (on a per unit basis) are the same throughout the network and that the angle difference across any line is close to 0. These are both safe assumptions for the system in steady state and necessary in a DC setting. The third assumption states that the resistance of every line is much less than its reactance, i.e. there are no losses. This assumption can be relaxed but for clarity of the derivation, we will keep it. Substituting these assumptions into equations (2.4) and (2.5),

$$W^n(\mathbf{s}, \mathbf{p}) = g_{nn} + \sum_{\substack{m=1 \\ m \neq n}}^N ([g_{nm} - b_{nm}(\theta^n - \theta^m)]) - (p^n - l^n) \quad (2.12)$$

$$f_\ell = h_\ell(\mathbf{s}) = b_\ell(\theta^i - \theta^j) \quad (2.13)$$

and by further applying the first assumption with Kirchhoffs first law, we can reduce equation (2.12) to:

$$W^n(\mathbf{s}, \mathbf{p}) = \sum_{\substack{m=1 \\ m \neq n}}^N (-b_{nm}(\theta^n - \theta^m)) - (p^n - l^n) \quad (2.14)$$

By forming a diagonal $L_{\mathcal{N}} \times L_{\mathcal{N}}$ matrix $\tilde{\mathbf{B}}$ (\mathcal{N} denotes the set of non zero-impedance branches) of the \tilde{b}_ℓ terms we can convert equations (2.13) and (2.14) to matrix notation ((2.16) and (2.17) respectively). The final $B\theta$ formulation is expressed as follows

$$\min_{\mathbf{p}, \theta} C(\mathbf{p}) \quad (2.15)$$

s.t.

$$\tilde{\mathbf{B}}\mathbf{A}_\tau\theta_\tau - \mathbf{f}_\tau = 0 \quad \forall \tau \quad (2.16)$$

$$\mathbf{A}'_\tau\mathbf{f}_\tau + \mathbf{p} - \mathbf{l} = 0 \quad \forall \tau \quad (2.17)$$

$$\underline{\mathbf{f}}_\tau \leq \mathbf{f}_\tau^{\mathcal{M}} \leq \bar{\mathbf{f}}_\tau \quad \forall \tau \quad (2.18)$$

$$\underline{\mathbf{p}} \leq \mathbf{p} \leq \bar{\mathbf{p}} \quad (2.19)$$

The superscript \mathcal{M} represents a monitored set of branches. Typically, system operators do not monitor every transmission branch for thermal violations. Operator experience dictates that many branches are very unlikely to bind and therefore do not need to be enforced in the OPF.

In the $B\theta$ formulation above we have included all contingency constraints explicitly in the OPF formulation. In real ED models only a subset of contingency constraints would be included directly in the formulation. Once an OPF solution is found using the subset, the resulting generation \mathbf{p} is used to calculate flows under the excluded contingent topologies using equations (2.17) and those flows would be validated using equation (2.18). Any excluded contingency flows that produced violations would be added into the original set of OPF constraints and the problem would be resolved. This iterative process would continue until no new violations are found. The external validation of flow limits in such a way is called contingency analysis and is a common approach used in actual markets. The inclusion of contingency constraints in an OPF is called the Security Constrained OPF (SCOPF) model.

To motivate the shift factor formulation in the next section we make a few observations about the $B\theta$ formulation. While solving this problem is significantly easier than the full AC model, for large systems with contingencies, the number of constraints will grow very quickly. In the case of PJM, there are approximately 6,000 contingency constraints that are included in the ED model. With 13,000+ busses and 20,000+ branches, we would have $6,000 \cdot 13,000$ nodal balance constraints and $6,000 \cdot 20,000$ flow equations. Even with modern solvers such a problem is difficult to solve. We need to find a way to reduce the number of constraints. In contingent topologies, for example, we only want to enforce the flow on a small number of branches and essentially ignore the flows on all other branches. The shift factor formulation allows us to do just that by working with sensitivity matrices. These matrices describe the impact of small changes in the system state on resulting power flow.

2.4 Shift Factor Formulation

A shift factor or injection shift factor (ISF) is defined as a linear approximation of the change in flow on line ℓ due to a change in injection at node n and a withdrawal at the reference bus (the reference bus corresponds to the column we removed from the incidence matrix). In this section we first derive an expression for the ISF and then apply it to formulate the shift factor OPF problem.

For a small change $\Delta \mathbf{p}$ and associated change in state, $\Delta \mathbf{s}$ we assume that $W(\mathbf{s} + \Delta \mathbf{s}, \mathbf{p} + \Delta \mathbf{p}) = \mathbf{0}$. In other words, a change in injection and resulting change to voltages and angles will continue to maintain the nodal balance constraints. Using this assumption in addition to the three assumptions from the $B\theta$ formulation and applying a first order Taylor's expansion about an initial state $\mathbf{0}$ we have

$$W(\mathbf{s}_0 + \Delta \mathbf{s}, \mathbf{p}_0 + \Delta \mathbf{p}) = W(\mathbf{s}_0, \mathbf{p}_0) + \left. \frac{\partial W}{\partial \mathbf{s}} \right|_{\mathbf{s}_0, \mathbf{p}_0} \Delta \mathbf{s} + \left. \frac{\partial W}{\partial \mathbf{p}} \right|_{\mathbf{s}_0, \mathbf{p}_0} \Delta \mathbf{p} + h.o.t \quad (2.20)$$

$$h(\mathbf{s}_0 + \Delta \mathbf{s}) = h(\mathbf{s}_0) + \left. \frac{\partial h}{\partial \mathbf{s}} \right|_{\mathbf{s}_0} \Delta \mathbf{s} + h.o.t = \mathbf{f}_0 + \left. \frac{\partial h}{\partial \mathbf{s}} \right|_{\mathbf{s}_0} \Delta \mathbf{s} + h.o.t \quad (2.21)$$

We consider both $\Delta \mathbf{p}$ and resulting $\Delta \mathbf{s}$ to be small and therefore ignore the higher order terms. It follows that

$$\left. \frac{\partial W}{\partial \mathbf{s}} \right|_{\mathbf{s}_0, \mathbf{p}_0} \Delta \mathbf{s} + \left. \frac{\partial W}{\partial \mathbf{p}} \right|_{\mathbf{s}_0, \mathbf{p}_0} \Delta \mathbf{p} \approx 0 \quad (2.22)$$

$$\Delta \mathbf{f} \approx \left. \frac{\partial h}{\partial \mathbf{s}} \right|_{\mathbf{s}_0} \Delta \mathbf{s} \quad (2.23)$$

From equation (2.14) it is clear that

$$\frac{\partial W}{\partial \mathbf{p}} = -\mathbf{I} \quad (2.24)$$

and by definition

$$\frac{\partial W}{\partial \mathbf{s}} = \left[\frac{\partial W}{\partial \theta} \quad \frac{\partial W}{\partial \mathbf{V}} \right] \quad (2.25)$$

By again examining equations (2.14) and (2.11) it is easy to see that

$$\frac{\partial W}{\partial \theta} \approx \mathbf{B} \quad (2.26)$$

and

$$\frac{\partial W}{\partial \mathbf{V}} \approx 0 \quad (2.27)$$

From equation (2.13) we see that for each branch $\ell = (i, j)$,

$$\frac{\partial h_\ell(\mathbf{s})}{\partial \theta} = \tilde{b}_\ell \quad \text{if } \theta = \theta^i \quad (2.28)$$

$$\frac{\partial h_\ell(\mathbf{s})}{\partial \theta} = -\tilde{b}_\ell \quad \text{if } \theta = \theta^j \quad (2.29)$$

$$\frac{\partial h_\ell(\mathbf{s})}{\partial \theta} = 0 \quad \text{otherwise} \quad (2.30)$$

In matrix notation this corresponds exactly to

$$\frac{\partial h}{\partial \mathbf{s}} = \tilde{\mathbf{B}}\mathbf{A} \quad (2.31)$$

Substituting these results back into equations (2.22) and (2.23) and observing that voltages do not appear anywhere in the state, we have

$$\mathbf{B}\Delta\mathbf{s} \approx \Delta\mathbf{p} \implies \Delta\mathbf{s} \approx \mathbf{B}^{-1}\Delta\mathbf{p} \quad (2.32)$$

$$\tilde{\mathbf{B}}\mathbf{A}\Delta\mathbf{s} \approx \Delta\mathbf{f} \quad (2.33)$$

Without proving this fact, the nodal susceptance matrix \mathbf{B} is invertible when the network is fully connected, i.e., there are no islands. We can now express the change in flow due to a change in injections as

$$\Delta\mathbf{f} \approx \tilde{\mathbf{B}}\mathbf{A}\mathbf{B}^{-1}\Delta\mathbf{p} \approx \boldsymbol{\Psi}\mathbf{p} \quad (2.34)$$

By our definition of the ISF at the beginning of this section we see that $\boldsymbol{\Psi}$ is in fact the injection shift factor matrix and tells us the change in flow on every line per unit change

in injection. We can now write the complete shift factor OPF problem as

$$\min_p C(p) \tag{2.35}$$

s.t

$$\mathbf{1}'(\mathbf{p} - \mathbf{1}) = 0 \tag{2.36}$$

$$\underline{\mathbf{f}}_\tau \leq \mathbf{f}_0 + \mathbf{\Psi}_\tau(\mathbf{p} - \mathbf{1}) \leq \bar{\mathbf{f}}_\tau \quad \forall \tau \tag{2.37}$$

$$\underline{\mathbf{p}} \leq \mathbf{p} \leq \bar{\mathbf{p}} \tag{2.38}$$

It is important to keep in mind that the shift factor formulation works with changes in injections from an initial state of the system. Under the assumption that $W(s + \Delta s, p + \Delta p) = 0$, we do not need to balance every bus in the system but only ensure that our new net injections are balanced in aggregate. This condition is given by constraint (2.36). With shift factors, we can directly attribute line flows to power sources and sinks. This means that we do not need to maintain a flow variable for every single branch but only monitor those branches that are expected to bind. Equation (2.37) ensures that flows on monitored branches are within their thermal ratings. While the shift factor matrix is topology dependent, the set of contingencies is known and all $\mathbf{\Psi}_\tau$'s can be pre-calculated. Further, under each contingent topology we can now monitor only the relevant branches, we do not need to restate all of the nodal balance and flow constraints as we did with the $B\theta$ formulation. In the next chapter we demonstrate the significant computational advantages of the shift factor formulation.

To end this section we introduce two additional sensitivity matrices that will be useful in the chapters that follow. Shift factor ψ_ℓ^m tells us the per-unit change in flow on branch ℓ due to an injection at node m and a withdrawal at the reference bus. Let us write the withdrawal at the reference bus explicitly:

$$\psi_\ell^m = \psi_\ell^m - \psi_\ell^N \tag{2.39}$$

Where the withdrawal at the reference bus has no impact of the flow of branch ℓ . Replacing the reference bus with another node, the difference between two shift factors is defined as

$$\phi_\ell^{m,n} = (\psi_\ell^m - \psi_\ell^N) - (\psi_\ell^n - \psi_\ell^N) = \psi_\ell^m - \psi_\ell^n \quad (2.40)$$

Similarly to equation (2.39) $\phi_\ell^{m,n}$ is the change in flow on branch ℓ due to an injection at bus m and withdrawal at bus n . The matrix Φ is called the power transfer distribution factor matrix (PTDF) and by taking the difference of two shift factors we eliminate the dependence on the reference bus. If busses m and n are the terminals of branch ℓ , we can write ϕ_ℓ^ℓ to denote the self-PTDF or the per-unit change in flow on branch ℓ due to an injection and withdrawal at its terminals. The self-PTDF of a radial branch, for example, is 1. The other matrix of interest is the line outage distribution factor matrix (LODF), \mathbf{O} . An LODF o_ℓ^k gives the sensitivity of branch ℓ flow with respect to a reduction in branch k flow, $o_\ell^k = -\partial f_\ell / \partial f_k$. The LODF o_ℓ^k is given by [13]

$$o_k^k = -1, \quad (2.41)$$

$$o_\ell^k = \frac{\phi_\ell^{m_k n_k}}{1 - \phi_k^{m_k n_k}}, \ell \neq k, \phi_k^{m_k n_k} \neq 1, \quad (2.42)$$

and is not defined for all $\ell \neq k$ if $\phi_k^{m_k n_k} = 1$, because the outage of such branches creates islands [14]

2.5 Shift Factor Formulation With Breakers

To formulate the shift factor OPF for a topology with breakers we need to extend the definition of shift factors. The shift factor matrix defined in equation (2.34) relies on the inverse of the nodal susceptance matrix, which in turn relies on line susceptances. Breakers, however, are characterized as zero-impedance connections, have an infinite susceptance and would lead to a non-invertible nodal susceptance matrix. To get around this problem we

start with a modified set of $B\theta$ constraints.²

$$\mathbf{f}_\tau^{\mathcal{N}} = \tilde{\mathbf{B}}_\tau^{\mathcal{N}} \mathbf{A}_\tau^{\mathcal{N}} \theta_\tau \quad (2.43)$$

$$\mathbf{A}_\tau^{\mathcal{Z}} \theta_\tau = \mathbf{0} \quad (2.44)$$

$$\mathbf{A}_\tau^{\mathcal{N}'} \mathbf{f}_\tau^{\mathcal{N}} + \mathbf{A}_\tau^{\mathcal{Z}'} \mathbf{f}_\tau^{\mathcal{Z}} = \mathbf{1} - \mathbf{p} \quad (2.45)$$

Equation (2.43) is the standard linearized equation for the flow of non-zero-impedance branches (denoted by superscript \mathcal{N}). For breakers the susceptance is infinity and (2.43) is undefined. Therefore, (2.44) enforces the condition that the voltage angle difference between the busbar endpoints is zero (denoted by superscript \mathcal{Z}). Equation (2.45) is the nodal balance constraint where we explicitly represent the flow on branches and breakers. To derive shift factor matrices associated with the topology describe above, we take derivatives with respect to the vector of nodal injections

$$\frac{d\mathbf{f}_\tau^{\mathcal{N}}}{d\mathbf{p}} = \frac{d\theta_\tau}{d\mathbf{p}} \mathbf{A}_\tau^{\mathcal{N}'} \tilde{\mathbf{B}}_\tau^{\mathcal{N}} \quad (2.46)$$

$$\frac{d\theta_\tau}{d\mathbf{p}} \mathbf{A}_\tau^{\mathcal{Z}'} = 0 \quad (2.47)$$

$$\frac{d\mathbf{f}_\tau^{\mathcal{N}}}{d\mathbf{p}} \mathbf{A}_\tau^{\mathcal{N}} + \frac{d\mathbf{f}_\tau^{\mathcal{Z}}}{d\mathbf{p}} \mathbf{A}_\tau^{\mathcal{Z}} = -\mathbf{I} \quad (2.48)$$

Substituting equation (2.46) into (2.48) gives

$$\frac{d\theta_\tau}{d\mathbf{p}} \mathbf{A}_\tau^{\mathcal{N}'} \tilde{\mathbf{B}}_\tau^{\mathcal{N}} \mathbf{A}_\tau^{\mathcal{N}} = -\left(\mathbf{I} + \frac{d\mathbf{f}_\tau^{\mathcal{Z}}}{d\mathbf{p}} \mathbf{A}_\tau^{\mathcal{Z}} \right) \quad (2.49)$$

or

$$\frac{d\theta_\tau}{d\mathbf{p}} = -\left(\mathbf{I} + \frac{d\mathbf{f}_\tau^{\mathcal{Z}}}{d\mathbf{p}} \mathbf{A}_\tau^{\mathcal{Z}} \right) \mathbf{B}_\tau^{-1} \quad (2.50)$$

The nodal susceptance matrix \mathbf{B}_τ in (2.50) is for the topology with all breakers open and is well defined as long as opening all candidate breakers does not create islands under any

²We skip the full derivation from AC equations having shown that the three linearization assumptions made in Chapter 1 reduce the AC OPF to the $B\theta$ one.

contingency τ . It may seem that enforcing non islanding conditions with all breakers open may be too restrictive. Note, however, that the OPF derivation in this section will be used in a topology control framework. Individual breakers within a substation are not generally of interest to system operators and such substations can be treated as a single node. In the chapter on substation reconfiguration, only candidate breakers, those that are of interest for topology control are represented explicitly and maintaining a connected system with them disconnected is more reasonable.

Returning to the derivation and substituting (2.50) into (2.47) gives

$$\boldsymbol{\Psi}_\tau^{\mathcal{Z}} = \left(\frac{d\mathbf{f}_\tau^{\mathcal{Z}}}{d\mathbf{p}} \right)' = - \left(\mathbf{A}_\tau^{\mathcal{Z}} \mathbf{B}_\tau^{-1} \mathbf{A}_\tau^{\mathcal{Z}'} \right)^{-1} \mathbf{A}_\tau^{\mathcal{Z}} \mathbf{B}_\tau^{-1} \quad (2.51)$$

Equation (2.51) defines the shift factor matrix for breakers as long as the inverse on the right hand side exists. The proof relies on two assumptions and is given by lemma 2.5.1

Lemma 2.5.1. *Given that there are no islands in the system with candidate breakers open under contingency τ , and when there are no closed loops formed by any set of breakers, matrix $\left(\mathbf{A}_\tau^{\mathcal{Z}} \mathbf{B}_\tau^{-1} \mathbf{A}_\tau^{\mathcal{Z}'} \right)^{-1}$ is invertible*

Proof. Under the no islands assumption, the nodal susceptance matrix is a positive definite, symmetric matrix [15], and therefore admits a Cholesky decomposition. Namely, $\mathbf{B}_\tau^{-1} = \mathbf{H}_\tau' \mathbf{H}_\tau$ and we can write

$$\begin{aligned} \mathbf{A}_\tau^{\mathcal{Z}} \mathbf{B}_\tau^{-1} \mathbf{A}_\tau^{\mathcal{Z}'} &= \mathbf{A}_\tau^{\mathcal{Z}} \mathbf{H}_\tau' \mathbf{H}_\tau \mathbf{A}_\tau^{\mathcal{Z}'} \\ &= \left(\mathbf{H}_\tau \mathbf{A}_\tau^{\mathcal{Z}'} \right)' \left(\mathbf{H}_\tau \mathbf{A}_\tau^{\mathcal{Z}'} \right) \end{aligned} \quad (2.52)$$

For notational purposes we assume $\mathbf{A}_\tau^{\mathcal{Z}}$ is a $k \times n$ matrix with $k < n$ (the number of breakers is less than the number of nodes in the network). If $\mathbf{A}_\tau^{\mathcal{Z}}$ is of maximal rank, k , then for any vector $v \neq 0$ it must be that $\left(\mathbf{A}_\tau^{\mathcal{Z}} \right)' v \neq 0$. Since \mathbf{H}_τ is, by definition,

non-singular $\mathbf{H}_\tau(\mathbf{A}_\tau^{\mathcal{Z}})'v \neq 0$ and

$$\left(\mathbf{H}_\tau \mathbf{A}_\tau^{\mathcal{Z}'} v\right)' \left(\mathbf{H}_\tau \mathbf{A}_\tau^{\mathcal{Z}'} v\right) \neq 0 \quad (2.53)$$

We therefore have

$$v' \mathbf{A}_\tau^{\mathcal{Z}} \mathbf{H}_\tau' \mathbf{H}_\tau \mathbf{A}_\tau^{\mathcal{Z}'} v = v' \left(\mathbf{A}_\tau^{\mathcal{Z}} \mathbf{B}_\tau^{-1} \mathbf{A}_\tau^{\mathcal{Z}'} \right) v \neq 0 \quad (2.54)$$

Which proves that the matrix product is invertible when $\mathbf{A}_\tau^{\mathcal{Z}}$ is of full rank. This will hold when there are no parallel breakers and when no subset of these breakers form a closed loop. Section 4.3 discusses how to transform $\mathbf{A}_\tau^{\mathcal{Z}}$ into a full rank matrix in the presence of loops or parallel breakers in the context of substation reconfiguration. \square

We can now express the shift factor matrix for non-zero-impedance branches by expanding equation (2.46) using (2.50)

$$\Psi_\tau^{\mathcal{N}} = \left(\frac{d\mathbf{f}_\tau^{\mathcal{N}}}{d\mathbf{p}} \right)' = -\tilde{\mathbf{B}}_\tau^{\mathcal{N}} \mathbf{A}_\tau^{\mathcal{N}} \mathbf{B}_\tau^{-1} \left(\mathbf{I} + \mathbf{A}_\tau^{\mathcal{Z}'} \left(\frac{d\mathbf{f}_\tau^{\mathcal{Z}}}{d\mathbf{p}} \right)' \right) \quad (2.55)$$

Equation (2.55) is the shift factor matrix for monitored branches where the first term on the right hand side,

$$\hat{\Psi} = -\tilde{\mathbf{B}}_\tau^{\mathcal{N}} \mathbf{A}_\tau^{\mathcal{N}} \mathbf{B}_\tau^{-1} \quad (2.56)$$

is the expression for the shift factor matrix with all candidate breakers open.

Applying the shift factors developed above we can formulate the OPF problem as follows

$$\min_p C(p) \quad (2.57)$$

s.t

$$\mathbf{1}'(\mathbf{p} - \mathbf{1}) = 0 \quad (2.58)$$

$$\underline{\mathbf{f}}_\tau^{\mathcal{M}} \leq \mathbf{f}_0 + \Psi_\tau^{\mathcal{M}}(\mathbf{p} - \mathbf{1}) \leq \bar{\mathbf{f}}_\tau^{\mathcal{M}} \quad \forall \tau \quad (2.59)$$

$$\underline{\mathbf{f}}_\tau^{\mathcal{Z}} \leq \mathbf{f}_0 + \Psi_\tau^{\mathcal{Z}}(\mathbf{p} - \mathbf{1}) \leq \bar{\mathbf{f}}_\tau^{\mathcal{Z}} \quad \forall \tau \quad (2.60)$$

$$\underline{\mathbf{p}} \leq \mathbf{p} \leq \overline{\mathbf{p}} \quad (2.61)$$

As noted above, the set \mathcal{Z} refers to the set of zero-impedance breakers connecting busbars of interest for TC. Typically there are no flow limits between busbars, constraint (2.60) is generally not included in OPF formulations, but we show it here for completeness.

In this section we derived a new shift factor based OPF model that incorporates breakers and branches. We show in later chapters that the shift factor based OPF is critical to our goal of solving the TC model in a reasonable time frame. The OPF derivation in this section is the first step toward that goal in the context of substation reconfiguration.

In the last section of this chapter we introduce the concept of locational marginal prices (LMPs). LMPs establish the price for energy purchases and sales at specific locations (nodes) throughout the wholesale electricity market and play an important role in TC applications. LMPs represent the locational value of energy and include the cost of energy and the cost of delivering it (losses and congestion).

2.6 LMPs in the Shift Factor OPF

By definition, the LMPs for the SCOPF formulated in problem (2.35)-(2.38) equal the derivative of the Lagrangian with respect to a change in nodal load [16]. Let the Lagrangian multipliers or shadow prices associated with constraints (2.36) and (2.37) be denoted by λ , $\underline{\boldsymbol{\mu}}$ and $\overline{\boldsymbol{\mu}}$, respectively. Using these shadow prices, the nodal prices $\boldsymbol{\pi}$ under the shift factor formulation are given by

$$\boldsymbol{\pi} = -(\lambda \mathbf{1} + \boldsymbol{\Psi}^{\mathcal{M}'}(\overline{\boldsymbol{\mu}} - \underline{\boldsymbol{\mu}})) \quad (2.62)$$

where $\boldsymbol{\Psi}^{\mathcal{M}}$ is a matrix that consist of the collection of $\boldsymbol{\Psi}_{\tau}^{\mathcal{M}}$, for all contingencies τ , respectively (the shadow prices $\underline{\boldsymbol{\mu}}$, $\overline{\boldsymbol{\mu}}$ have as elements the corresponding shadow prices for each contingency). As mentioned in the previous section the LMP reflects the cost of energy and its delivery. The shadow price λ reflects the cost of energy. In the absence of

congestion, everyone would pay the same price for energy (we exclude losses in the OPF formulation for now). When transmission constraints are binding, i.e. congestion exists, some of the shadow prices $\underline{\mu}, \bar{\mu}$ will be non zero and we can think of the transpose to the shift factor matrix, Ψ' as allocating the congestion cost of constraints to individual nodes. LMPs provide valuable information in the context of topology control. For example, it is common and should come as no surprise that power flows from low price to high price locations. If we observe the opposite behavior where power flows on a branch against the price, we say that the flow is uneconomic and this presents an opportunity for topology control. In large scale systems attempting to consider every branch in a TC optimization is impractical. In [17], for example, the authors apply policies such as the LMP difference between branch terminals to limit the set of potentially promising branches. We will not discuss these policies further in this work but only highlight that LMPs play a critical role in the market and return to them in the next chapter in the context of topology control.

Chapter 3

Topology Control - Branch Switching

This chapter develops the shift factor based topology control formulation. We start with some background and discussion of previous $B\theta$ TC models and then introduce flow cancelling transactions (FCTs), the main tool for dynamic modeling of line outages within a shift factor framework. While flow cancelling transactions have been used in other applications, e.g. [14] their application here in a MIP setting allows for a novel approach to shift factor based topology control. After developing both formulations, the chapter focuses on implementation aspects and numerical experience on a large system. Lastly, we discuss extensions of the shift factor TC formulation to include losses and AC-modeling (not to be confused with solving an AC OPF).

3.1 $B\theta$ Topology Control Formulation

The typical MILP formulations of topology control problems model transmission flows using (2.16), i.e., explicitly keeping the susceptances as inputs and voltage angles as decision variables [10–12, 18], hence the name $B\theta$ formulation. The supply-demand balance is enforced at the nodal level using (2.17). The reason for choosing the model is that the linear inclusion of binary variables associated with the connection or disconnection of branches is more intuitive than in the shift factor model, which has a nonlinear dependence on susceptances and connectivity (2.37).

For notational simplicity, and without loss of generality, assume there is at most one generator at each bus, which has a constant marginal cost. The SCOPF with TC minimizes

generator costs to serve load (3.1) subject to physical constraints such as generator (3.2) and branch (3.3) limits. The incorporation of TC requires the addition of a binary variable (3.7), which renders the problem an MILP. The power balance at each bus is enforced by (3.4). In addition, (3.5) and (3.6) define flows as a function of voltage angles, where M is a sufficiently large number and the first two terms are from (2.16). Note that this formulation computes angles for all buses and flows on all branches for each contingency τ of a pre-specified contingency list. Selected topology changes due to controlled actions are specified by the 0/1 (open/closed) status of the set of branches whose status is controllable, indicated by vector \mathbf{z} . Together, contingent topologies represented by index τ and dynamic changes controlled by \mathbf{z} define a transmission topology.

$$\mathcal{C} = \min_{\mathbf{p}, \boldsymbol{\theta}, \mathbf{f}, \mathbf{z}} \mathbf{c}'_p \mathbf{p} \quad (3.1)$$

$$\text{subject to} \quad \underline{\mathbf{p}} \leq \mathbf{p} \leq \bar{\mathbf{p}} \quad (3.2)$$

$$\tilde{\mathbf{F}}_\tau \mathbf{z} \leq \mathbf{f}_\tau \leq \tilde{\bar{\mathbf{F}}}_\tau \mathbf{z} \quad \forall \tau \quad (3.3)$$

$$\mathbf{A}'_\tau \mathbf{f}_\tau + \mathbf{p} - \mathbf{1} = 0 \quad \forall \tau \quad (3.4)$$

$$\tilde{\mathbf{B}} \mathbf{A}_\tau \boldsymbol{\theta}_\tau - \mathbf{f}_\tau + (\mathbf{1} - \mathbf{z}) M \geq 0 \quad \forall \tau \quad (3.5)$$

$$\tilde{\mathbf{B}} \mathbf{A}_\tau \boldsymbol{\theta}_\tau - \mathbf{f}_\tau + (\mathbf{1} - \mathbf{z}) M \leq 0 \quad \forall \tau \quad (3.6)$$

$$z_\ell \in \{0, 1\} \quad \forall \ell \quad (3.7)$$

In the remainder of this work, problem (3.1)-(3.7) is referred to as the *B θ TC formulation*. Let the number of generators be G , the number of contingencies be T and the number of switchable branches be S . The *B θ TC* formulation has approximately $G + (N - 1)T + LT + S$ decision variables and $2G + 4LT + NT + S$ constraints, and the number of non-zero values is $o((L + N)T)$. As such, the problem dimension is essentially insensitive to the number of switchable branches and monitored transmission constraints.

For example, the standard *B θ TC* model size explodes with security constraints: the

optimal power flow (OPF) model with TC on the IEEE 118-bus test system with $N - 1$ security constraints (a system is said to be $N - 1$ secure if it can withstand any single contingency and still supply all demand without violations) requires 63,000 variables and 200,000 constraints, compared to approximately 500 variables and 1000 constraints in the absence of contingency analysis [11]. In terms of solution time, its performance is prohibitively slow: the integrality gap of the security-constrained OPF (SCOPF) with TC was about 60% after six days of run time [11]. While there have been significant improvements in MILP solvers and computer resources since the publication of [11], and while formulations have been improved with the addition of symmetry breaking and anti-islanding constraints [17, 19], the resulting computation times are still very far from the required times for operational deployment in real systems.

To overcome computational tractability issues, heuristic approaches have been developed for the TC problem. Some of these heuristics use the $B\theta$ MILP formulation [11], but the reduction in computational effort is not sufficient for practical applications. Alternative approaches based on sensitivity analysis have been very successful in reducing computational times in an OPF setting, where dispatch is optimized for a single time period [17, 20–22]. However, the extension of these tractable approaches to a dynamic setting (e.g., multi-interval ED and UC) is not trivial. Intertemporal constraints, such as maximum number of breakers that can change state on a given interval and maximum switching frequencies, combined with other constraints such as the total number of breakers that can be open at any point in time all require topology optimization over a multiple time period horizon.

3.2 Shift Factor Topology Control Formulation

We stated earlier that the inclusion of topology control in the shift factor formulation is not intuitive due to the nonlinear dependence of binary decision variables on susceptances and connectivity. To motivate the use of flow cancelling transactions that allow us to maintain

a linear shift factor based MIP, we first show where the straightforward approach leads us to a nonlinear formulation. Consider a transaction (i_s, j_s, u) denoting an injection of u MW at *from* node i_s of branch s and a withdrawal at the *to* node, j_s of branch s . The change in flow on branch ℓ due to transaction (i_s, j_s, u) is given by applying the PTDF

$$\Delta f_\ell = \phi_\ell^{(i_s, j_s, u)} u = \left(\psi_\ell^{i_s} - \psi_\ell^{j_s} \right) u \quad (3.8)$$

and the change in flow on line ℓ per unit of flow on branch s after branch s is disconnected is expressed using the LODF

$$\frac{\Delta f_\ell^{(-s)}}{f_s} = LODF_\ell^s = \frac{\phi_\ell^{(i_s, j_s, 1)}}{1 - \phi_s^{(i_s, j_s, 1)}} \quad (3.9)$$

Where the superscript $(-s)$ denotes the disconnection of branch s . Using (3.9), the change in flow on branch ℓ after s is disconnected is

$$\Delta f_\ell^{(-s)} = \frac{\psi_\ell^{i_s} - \psi_\ell^{j_s}}{1 - \left(\psi_s^{i_s} - \psi_s^{j_s} \right)} f_s \quad (3.10)$$

By definition of shift factors, the flow on branches s and ℓ before s is disconnected are

$$f_s = f_s^0 + \psi_s(\mathbf{p} - \mathbf{1}) \quad \text{and} \quad (3.11)$$

$$f_\ell = f_\ell^0 + \psi_\ell(\mathbf{p} - \mathbf{1}) \quad (3.12)$$

Where f^0 denotes the base flow in the full topology. Combining (3.10) and (3.11) we can write the change in flow on branch ℓ as a function of nodal injections

$$\begin{aligned} f_\ell^{(-s)} &= f_\ell + \Delta f_\ell^{(-s)} = f_\ell^0 + \psi_\ell(\mathbf{p} - \mathbf{1}) + \frac{\psi_\ell^{i_s} - \psi_\ell^{j_s}}{1 - \left(\psi_s^{i_s} - \psi_s^{j_s} \right)} \psi_s(\mathbf{p} - \mathbf{1}) = \\ &= f_\ell^0 + \left[\psi_\ell + \frac{\phi_\ell^{(i_s, j_s, 1)}}{1 - \left(\psi_s^{i_s} - \psi_s^{j_s} \right)} \psi_s \right] (\mathbf{p} - \mathbf{1}) \end{aligned} \quad (3.13)$$

Note that equation (3.13) is of the same form as the standard shift factor flow equation where we have defined the shift factor matrix in the topology with branch s disconnected in terms of the full topology sensitivity matrices

$$\psi_l^{(-s)} = \boldsymbol{\psi}_l + \frac{\phi_l^{(i_s, j_s, 1)}}{1 - (\psi_s^{i_s} - \psi_s^{j_s})} \boldsymbol{\psi}_s \quad (3.14)$$

Using the notation of $z_s = 1$ to denote that line s is connected and $z_s = 0$ to denote that it is disconnected we can express the change in ISF conditional on the opening of line s :

$$\Delta \boldsymbol{\psi}_l | z_s = \frac{\phi_l^{(i_s, j_s, 1)}}{1 - (\psi_s^{i_s} - \psi_s^{j_s})} \boldsymbol{\psi}_s (1 - z_s) \quad (3.15)$$

We can see that using this ISF directly in an OPF formulation would make the formulation non-linear since: $[\Delta \boldsymbol{\psi}_l | z_s] (\mathbf{p} - \mathbf{1})$ is not linear in the decision variables z_s, \mathbf{p} .

We have shown that attempting to update the shift factor matrix explicitly within the original shift factor OPF leads to a nonlinear formulation and are ready to introduce flow cancelling transaction.

Flow-cancelling transactions provide an alternative approach that apply a power transfer across the outaged branch (without opening it) that results in the same changes in all remaining branch flows, so that from the point of view of the rest of the system, the branch is outaged

3.2.1 Flow-Cancelling Transactions

Flow cancelling transactions (FCTs) are virtual transaction, pairs of injections and withdrawals at the ends of opened lines, that drives the total flow through the *interface* between the branch and the rest of the system to zero. The modeling approach of representing outages as a flow-cancelling transaction is widely known, for example, as a tool to derive line outage distribution factors [13].

To model the outage of line $k = (m, n)$, which does not island the system, let m'_k and n'_k

be infinitely close to the terminal buses m_k and n_k along line k (Fig. 3.1). Let there be a transaction from m'_k to n'_k whose magnitude $v_{k\tau}$ is such that the impact of the transaction on the rest of the system is equivalent to the opening of line k . To meet this condition, the flow-cancelling transaction must make the flow on the interface between the rest of the system and line k , i.e., each of the infinitesimally short lines m'_k to m_k and n'_k to n_k , to be zero. Using the PTDF definition,

$$f_{k\tau} - \left(1 - \phi_{k\tau}^{m'_k n'_k}\right) v_{k\tau} = 0. \quad (3.16)$$

Hence,

$$v_{k\tau} = \frac{f_{k\tau}}{1 - \phi_{k\tau}^{m'_k n'_k}}. \quad (3.17)$$

The flow-cancelling transaction is well defined, since $\phi_{k\tau}^{m'_k n'_k} \neq 1$ when the non-islanding assumption holds [14]. The vector of flow-cancelling transactions that model the outage of

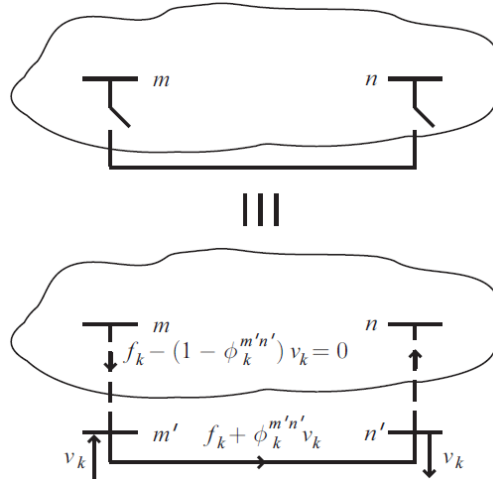


Figure 3.1: Opening line k (top) is equivalent from the point of view of the rest of the system as inserting a flow-cancelling transaction at virtual buses m' and n' , infinitely close to m and n , respectively, and along line k (bottom).

a (non-islanding) set \mathcal{S} of lines can be obtained by applying the principle of superposition,

i.e., by enforcing condition (3.16) for all lines in the set [23],

$$\mathbf{f}_\tau^{\mathcal{S}} - (\mathbf{I} - \Phi_\tau^{\mathcal{S}\mathcal{S}}) \mathbf{v}_\tau^{\mathcal{S}} = \mathbf{0}. \quad (3.18)$$

The superscript \mathcal{S} identifies the vectors of variables associated to set \mathcal{S} , and $\Phi_\tau^{\mathcal{S}\mathcal{S}}$ is the matrix of PTDFs for transactions between the terminal points of lines in \mathcal{S} , with respect to the flows of lines in \mathcal{S} . Note that, even if there are identical parallel lines, the rows corresponding to these lines in (3.18) are not identical.¹ In fact, as long as there is no islanding, (3.18) has a unique solution $\mathbf{v}_\tau^{\mathcal{S}}$. Under islanding conditions, network flows are not well-defined without additional equations enforcing power balance in each island.²

The utilization of flow-cancelling transactions allows us to formulate a new shift factor based MILP formulation for topology control that we discuss in the next section.

3.2.2 FCT MIP Formulation of Topology Control

Let the superscript \mathcal{S} denote variables or parameters related to branches in the switchable set. For each contingency τ , let \mathbf{v}_τ be the vector of flow-cancelling transactions to model the state of all switchable branches, $\Psi_\tau^{\mathcal{S}}$ be the shift factor matrix associated to switchable branches, and $\Phi_\tau^{\mathcal{S}\mathcal{S}}$ be the self-PTDF matrix of the switchable set. For the closed switchable branches, (2.33) needs to be enforced with appropriate limits, similar to (3.3). For the open switchable branches, (3.18) needs to be enforced in addition to (2.33). This is achieved through additional constraints,

$$\underline{\mathbf{f}}_\tau^{\mathcal{S}} \mathbf{z} \leq \Psi_\tau^{\mathcal{S}} (\mathbf{p} - \mathbf{1}) + (\Phi_\tau^{\mathcal{S}\mathcal{S}} - \mathbf{I}) \mathbf{v}_\tau \leq \bar{\mathbf{f}}_\tau^{\mathcal{S}} \mathbf{z}, \quad \forall \tau \quad (3.19)$$

$$-M(\mathbf{1} - \mathbf{z}) \leq \mathbf{v}_\tau \leq M(\mathbf{1} - \mathbf{z}), \quad \forall \tau, \quad (3.20)$$

¹Indeed, the diagonal entry in $(\mathbf{I} - \Phi_\tau^{\mathcal{S}\mathcal{S}})$ corresponding to the line of interest is 1 minus the line self-PTDF, while for any other identical line, the entry in the same row is the PTDF of the flow-cancelling transaction across the line of interest on the parallel line.

²If \mathcal{S} is islanding, there are infinite $\mathbf{v}_\tau^{\mathcal{S}}$ that meet (3.18) but these flow-cancelling transactions may not represent islanded operation.

where \mathbf{z} indicates the state of the branches, as in Section 3.1. For a sufficiently large M , constraints (3.20) force the flow-cancelling transactions to be 0 for all closed branches, while allowing them to be unrestricted for all open branches (the magnitude of M is discussed in Section 3.2.4).

The flow-cancelling transaction \mathbf{v}_τ^S is a function of the contingency τ as well as the selected state \mathbf{z} of switchable branches, in the same way that angles $\boldsymbol{\theta}_\tau$ in (3.5-3.6) depend on \mathbf{z} and τ . That is, with contingency constraints, each flow-cancelling transaction is represented by a set of magnitudes: one for the base case and one for each contingency, and all of these magnitudes depend on the selected \mathbf{z} . Opening a branch requires different flow-cancelling transactions under different topologies induced by the outage of contingency branches.

Let variables and parameters related to monitored but not switchable branches be denoted with superscript \mathcal{M} (in the remainder of the work, a monitored branch means a monitored branch that is not switchable, as all switchable branches are explicitly included in the problem formulation, and thus monitored). Let $\boldsymbol{\Psi}_\tau^{\mathcal{M}}$ be the reduced shift factor matrix associated with monitored branches under contingency topology τ , and $\boldsymbol{\Phi}_\tau^{\mathcal{MS}}$ be the PTDF matrix of transactions between the terminal buses of each switchable branch with respect to branches in the monitored set, under topology τ . For monitored branches, the flow constraints incorporate the impacts of flow-cancelling transactions for switchable branches, and are given by

$$\underline{\mathbf{f}}_\tau^{\mathcal{M}} \leq \boldsymbol{\Psi}_\tau^{\mathcal{M}} (\mathbf{p} - \mathbf{1}) + \boldsymbol{\Phi}_\tau^{\mathcal{MS}} \mathbf{v}_\tau \leq \bar{\mathbf{f}}_\tau^{\mathcal{M}} \quad \forall \tau. \quad (3.21)$$

The resulting formulation of the SCOPF with TC is

$$\mathcal{C} = \min_{\mathbf{p}, \mathbf{v}, \mathbf{z}} \mathbf{c}'_p \mathbf{p} \quad (3.22)$$

$$\text{s.t. } \mathbf{1}' (\mathbf{p} - \mathbf{1}) = 0 \quad (3.23)$$

$$\underline{\mathbf{p}} \leq \mathbf{p} \leq \bar{\mathbf{p}} \quad (3.24)$$

$$\underline{\mathbf{f}}_\tau^{\mathcal{M}} \leq \Psi_\tau^{\mathcal{M}} (\mathbf{p} - \mathbf{1}) + \Phi_\tau^{\mathcal{M}\mathcal{S}} \mathbf{v}_\tau \leq \bar{\mathbf{f}}_\tau^{\mathcal{M}} \quad \forall \tau \quad (3.25)$$

$$\underline{\mathbf{f}}_\tau^{\mathcal{S}} \mathbf{z} \leq \Psi_\tau^{\mathcal{S}} (\mathbf{p} - \mathbf{1}) + (\Phi_\tau^{\mathcal{S}\mathcal{S}} - \mathbf{I}) \mathbf{v}_\tau \leq \bar{\mathbf{f}}_\tau^{\mathcal{S}} \mathbf{z} \quad \forall \tau \quad (3.26)$$

$$-M (\mathbf{1} - \mathbf{z}) \leq \mathbf{v}_\tau \leq M (\mathbf{1} - \mathbf{z}) \quad \forall \tau \quad (3.27)$$

$$z_\ell \in \{0, 1\} \quad \forall \ell \quad (3.28)$$

Problem (3.22)-(4.16), referred to as the *shift factor TC formulation*, is equivalent to the $B\theta$ formulation in the sense that both yield the same optimal solution as long as the transmission constraints that bind in the $B\theta$ formulation are modeled in the shift factor formulation. However, problem size and complexity are quite different. The shift factor TC formulation has $G + TZ + Z$ decision variables and $1 + 2G + 2C + 4TZ + Z$ constraints, where C is the number of monitored/contingency pairs. The number of non-zero problem entries is $o((N + Z)(C/T + Z)T)$. If the number of switchable branches and monitored/contingency pairs are relatively small, the shift factor formulation is significantly smaller than the $B\theta$ formulation in every sense. As the number of switchable, monitored and contingency branches becomes sufficiently large, the number of non-zero elements in the shift factor formulation becomes larger than in the $B\theta$ TC formulation, although the number of constraints always remains smaller in the shift factor formulation, as there is just a single power balance equation.

3.2.3 LMPs under the FCT MIP

While the shift factor TC formulation is consistent with standard SCOPF formulations used in nodal markets, there are additional constraints (3.26) that require modifications to the standard locational marginal price (LMP) expressions used in the markets. This section determines these modifications, and shows how the LMPs in the shift factor TC formulation can be equivalently expressed in the usual form as the LMPs of a SCOPF (without TC) for the optimal \mathbf{z} .

The LMPs for the standard SCOPF were derived in section 2.6. With topology control

we introduce Lagrangian multipliers $\underline{\alpha}$ and $\bar{\alpha}$ for the new constraints (3.26). Using these shadow prices, the nodal prices $\boldsymbol{\pi}$ under the shift factor TC formulation are given by

$$\boldsymbol{\pi} = -(\lambda \mathbf{1} + \boldsymbol{\Psi}^{\mathcal{M}'}(\bar{\boldsymbol{\mu}} - \underline{\boldsymbol{\mu}}) + \boldsymbol{\Psi}^{\mathcal{S}'}(\bar{\boldsymbol{\alpha}} - \underline{\boldsymbol{\alpha}})) \quad (3.29)$$

where $\boldsymbol{\Psi}^{\mathcal{S}}$ and $\boldsymbol{\Psi}^{\mathcal{M}}$ are matrices that consist of the collection of $\boldsymbol{\Psi}_{\tau}^{\mathcal{S}}$ and $\boldsymbol{\Psi}_{\tau}^{\mathcal{M}}$, for all contingencies τ , respectively (as do the shadow prices $\underline{\boldsymbol{\mu}}$, $\bar{\boldsymbol{\mu}}$, $\underline{\boldsymbol{\alpha}}$ and $\bar{\boldsymbol{\alpha}}$).

In order to gain intuition with respect to (3.29), let us consider the optimal (base) topology derived from the solution $\mathbf{z} = \mathbf{z}^*$ of (3.22)-(3.28). Also, let us relabel ex-post any switchable branches which remain closed in the optimal topology as monitored (including relabeling as elements of $\underline{\boldsymbol{\mu}}$ and $\bar{\boldsymbol{\mu}}$ the terms of $\underline{\boldsymbol{\alpha}}$ and $\bar{\boldsymbol{\alpha}}$, respectively, associated to these closed switchable branches). The shift factor matrix for the optimal topology \mathbf{z}^* is given in [13] as

$$\boldsymbol{\Psi}^{\mathcal{M}^*} = \boldsymbol{\Psi}^{\mathcal{M}} + \mathbf{O}^{\mathcal{MS}} \boldsymbol{\Psi}^{\mathcal{S}} \quad (3.30)$$

where $\mathbf{O}^{\mathcal{MS}}$ is the LODF matrix indicating the impact of switched branch outages on monitored branches for each contingency. In addition, the LMPs for the optimal topology \mathbf{z}^* are defined in the standard manner (see [13]), as

$$\boldsymbol{\pi}^* = -(\lambda^* \mathbf{1} + \boldsymbol{\Psi}^{\mathcal{M}^*'}(\bar{\boldsymbol{\mu}}^* - \underline{\boldsymbol{\mu}}^*)) \quad (3.31)$$

For the optimal topology \mathbf{z}^* the SCOPF with TC and the SCOPF without TC yield equivalent solutions so that the LMPs (3.32) and shadow prices associated with flow limits on transmission elements (3.33) must also be equivalent:

$$\boldsymbol{\pi} = \boldsymbol{\pi}^* \quad (3.32)$$

$$\underline{\boldsymbol{\mu}} = \underline{\boldsymbol{\mu}}^* \quad (3.33)$$

Substituting (3.29) and (3.31) into (3.32), and canceling the energy component yields,

$$\Psi^{\mathcal{M}'}(\underline{\bar{\mu}} - \underline{\mu}) + \Psi^{\mathcal{S}'}(\underline{\bar{\alpha}} - \underline{\alpha}) = \Psi^{\mathcal{M}'*}(\underline{\bar{\mu}}^* - \underline{\mu}^*) \quad (3.34)$$

Furthermore, substituting (3.30) and (3.33) and appropriately canceling like terms yields,

$$\underline{\bar{\alpha}} - \underline{\alpha} = \mathbf{O}^{\mathcal{MS}'}(\underline{\bar{\mu}} - \underline{\mu}) \quad (3.35)$$

Based on [20], the shadow prices $\underline{\bar{\alpha}} - \underline{\alpha}$ are interpreted as (minus) the total derivative of the generation costs with respect to reducing flow on the (opened) switchable branches. If the difference in shadow prices is positive, reducing flow on the “candidate” branch will reduce generation costs. Of course with topology control we cannot reduce the flow in the marginal sense but only fully disconnect the branch, however, this metric can serve as one indicator of branches to consider for topology control. Finally, by substituting (3.35) into (3.29) we see that the LMP (3.29) derived from the SCOPF with TC can be expressed in the standard form as

$$\pi = -(\lambda \mathbf{1} + (\Psi^{\mathcal{M}} + \mathbf{O}^{\mathcal{MS}} \Psi^{\mathcal{S}})'(\underline{\bar{\mu}} - \underline{\mu})) \quad (3.36)$$

3.2.4 Formulation Implementation Aspects

This section discusses bounds on M , a method for fast islanding conditions detection, and contingency constraint modeling. These are issues of practical importance in the implementation of the shift factor TC formulation, for computational and data management reasons.

In the shift factor TC formulation, the only parameter left without a precise value is M , defined simply as a *sufficiently large number*. From (3.17), $v_{k\tau} = f_k + \phi_{k\tau}^{m'n'} v_{k\tau}$. Thus, the value of the flow-cancelling transaction is equal to the flow on branch k when the angle difference between its terminals is equal to the angle difference that occurs when the

branch is opened (for an illustration, refer to Fig. 3.1). Hence, if branch k is open, for any contingency topology τ the following holds (as long as there is no islanding):

$$v_{k\tau} = \tilde{b}_k \mathbf{A}_{k\tau} \boldsymbol{\theta}_\tau. \quad (3.37)$$

From (3.37), we can see that M can be bounded by the maximum potential value of the product of the branch susceptance and angle difference. Indeed,

$$\max_{k,\tau} (v_{k\tau}) = \max_{k,\tau} (\tilde{b}_k \mathbf{A}_{k\tau} \boldsymbol{\theta}_\tau) \quad (3.38)$$

$$\leq \max_k (\tilde{b}_k) \max_{k,\tau} (\mathbf{A}_{k\tau} \boldsymbol{\theta}_\tau) \quad (3.39)$$

$$= M, \quad (3.40)$$

where $\mathbf{A}_{k\tau}$ is the row in \mathbf{A}_τ corresponding to branch k . Note that this same bound is applicable for setting the M value in the $B\theta$ formulation, since $f_k = 0$ when $z_k = 0$, so that the M value from (3.40) ensures that (3.5) and (3.6) are met.

Under normal conditions, islanding operation is undesirable, leading to incorrect description of constraints and possibly reliability concerns. As such, fast islanding detection, both for the normal state and for all contingency states, is important when change of the transmission topology is contemplated. As in the previous section, let us relabel ex-post any switchable branches which remain closed in the optimal topology as monitored. Using results in [14], islanding can be detected quickly by evaluating the singularity of matrices $(\boldsymbol{\Phi}_\tau^{SS} - \mathbf{I})$ for all contingencies τ . Note that these matrices are already available. Also, while the number of such matrices could be non-trivial, the matrices are relatively small, with size equal to the number of branches opened in the optimal topology. Finally, the singularity evaluations can be done in parallel, further speeding the analysis.

In (3.25), the flows under each contingency τ are modeled using different shift factor matrices $\boldsymbol{\Psi}_\tau^M$ and $\boldsymbol{\Phi}_\tau^{MS}$. An alternative approach that does not require a separate shift factor matrix calculation under each topology is to model the occurrence of contingencies

using flow-cancelling transactions, in the same way that controlled topology changes are modeled, and along the lines of [24]. Doing so internalizes the shift factor calculations for each contingency. The computational time effects of such approach have not been analyzed, although we expect that the original implementation would solve faster, since it requires fewer constraints and decision variables. However, if the set of relevant contingency constraints is not known in advance, internalizing the shift factor updates may be attractive due to its simpler data management requirements, and potentially comparable solution times (once shift factor update times are accounted for).

3.3 Numerical Experience on a Large System

The shift factor TC formulation was previously compared against the $B\theta$ TC formulation using the IEEE 118-bus test system in [25]. Analysis of a wide range of switchable sets, varying from no switchable branches to 24 switchable branches (i.e., over 12% of the 194 branches in the system) yielded that the shift factor TC formulation has lower computational times for all switchable set sizes analyzed. However, the computational savings were more significant for smaller switchable sets, as expected due to the dependence of the shift factor formulation size on the cardinality of the switchable set.

In this section we compare the performance of both formulations using a large-scale, real system model. The model represents in detail the conditions seen by PJM of both its footprint as well as the neighboring areas on June 23, 2010 at 8:30 am. This interval was selected based on the average results obtained on it when applying tractable TC policies such as those in [17]. The underlying topology, load, losses, interchange and unit commitment are as archived by the PJM EMS for the 5-minute interval starting at 8:30 and ending at 8:35 am. Generation economic and constraint data are from the PJM real-time market for the simulated day. The model has 857 dispatchable PJM generators and 2267 non-dispatchable/fixed generators (including all units outside of PJM), 13,436 buses and 18,415 branches. Constraints enforced are all no-contingency or single-contingency

monitored constraints in the PJM real-time markets for at least one interval during the week of June 20-26, 2010. Thirty contingency constraints were considered on top of the 156 base case constraints (no-contingency state of the transmission system). The 30 contingency constraints include 20 different contingencies (there are some constraints that share the same contingency).

Both TC formulations were implemented in AIMMS 3.12 using CPLEX 12.5. Simulations were run on a 64-bit workstation with two 2.93 GHz Intel Xeon processors (8 cores total) and 24 GB of RAM. The convergence criterion was an optimality gap tolerance of 0.05%. A value of 5000 was used for M in both formulations and a time limit of 1 hour was used for all simulations.

The TC formulations implemented and tested include two sets of constraints not detailed in the previous sections. We added connectivity constraints that ensure that each generator and load bus is connected by at least two lines, and symmetry-breaking constraints that provide a preferred ordering for each group of identical parallel lines.

Two sets of cases were evaluated, with and without contingency constraints and each case was also solved without TC to provide a benchmark. Twenty switchable lines were considered, selected using sensitivity metrics [17]. For each case, we ran 20 samples in a Monte Carlo type of analysis. In each sample we maintain a fixed load and perform a Monte Carlo simulation where the fuel costs and the available wind generation are randomly varied. Fuel costs are assumed to be uniformly distributed and to meet the condition that the cost of coal is lower than the cost of natural gas, which in turn is lower than the cost of fuel oil. Available capacity of the wind plants is assumed to be uniformly distributed between 0 and their rated capacity.

For the $B\theta$ formulation we evaluated the default Dual Simplex method as well as the Barrier method available in CPLEX for solving the LP subproblems of the MIP.

Table 3.1 summarizes solutions time statistics across the 20 samples, reported in seconds, for the cases without TC (using the CPLEX LP solver). The abbreviation DS refers to the Dual Simplex method used by default in CPLEX and BR refers to the Barrier

method. As seen from the table above, the shift factor (Ψ) formulation solves significantly

Table 3.1: LP Formulation Results

	Without Contingencies			With Contingencies		
	$B\theta$ - DS	$B\theta$ - BR	Ψ	$B\theta$ - DS	$B\theta$ - BR	Ψ
Avg.	0.65	0.54	0.12	37.28	80.24	.67
Min.	0.42	0.50	0.06	14.49	26.80	0.64
Max.	0.91	0.62	0.14	74.37	541.09	0.70
Sum.	12.95	10.86	2.32	745.68	1,604	13.48
sDev.	0.13	0.03	0.02	14.31	129.69	0.02

faster than the $B\theta$ formulation. For the $B\theta$ formulation, the Barrier method performs better for the small case without contingencies but for the large case becomes more unstable. Specifically, for two of the samples under the $B\theta$ -BR method the solution time were significantly larger than for all other samples (351 and 541 seconds respectively). If these times are excluded from the statistics of table 3.1, the minimum time and standard deviation is still higher compared to the $B\theta$ -DS method but the average and max times are very similar. Despite the sparsity of the $B\theta$ formulation, the significant increase in variables and constraints (shown in table 3.2) results in much slower solution times. The

Table 3.2: Constraint and Variable Statistics – LP Case with Contingencies

Variables	$B\theta$	Ψ
Flow	386,715	0
Voltage Angle	282,156	0
Generator	857	857
Total	669,728	857
Constraints	$B\theta$	Ψ
Flow Limits (2x)	586	586
Kirchhoff	386,715	0
Nodal Balance	282,156	1
Generation Limits (2x)	857	857
Total	671,757	2,886
Matrix Density (%)	0.0036%	21.28%

compactness of the shift factor formulation, detailed in table 3.2, clearly outweighs the sparsity of the $B\theta$ formulation in terms of solver performance, especially for the more re-

alistic case with contingency constraints. Table 3.3 show solution time statistics³ when we introduce 20 switchable branches into both formulation. For the cases with 20 switchable

Table 3.3: MIP Formulation Results

	Without Contingencies			With Contingencies		
	$B\theta$ - DS	$B\theta$ - BR	Ψ	$B\theta$ - DS	$B\theta$ - BR	Ψ
Avg.	26.80	29.24	0.57	3,157	3,352	6.98
Min.	2.76	5.12	0.56	1,406	186.73	5.13
Max.	107.67	85.72	0.58	3,926	3,864	9.36
Sum.	535.91	584.72	11.31	50,521	67,054	139.59
sDev.	30.81	22.20	0.006	743.09	924.44	1.01

lines the $B\theta$ formulation becomes impractical. Even with few contingencies modeled (30 contingencies represent less than 0.2% of the total number of branches) and despite the clear advantage in terms of sparsity, solve times for $B\theta$ make it unusable in both operation and market settings. Not only is the $B\theta$ method significantly slower than the shift factor formulation, it also performs worse in terms of production cost savings. In 12 samples, the shift factor formulation achieves a better MIP gap but more importantly, the shift factor formulation always reaches the MIP gap tolerance where the $B\theta$ formulation does not reach the tolerance within the 1 hour time limit in 4 samples (sometimes stopping at as high as 3.7%).

Several assumptions used in this section can be easily relaxed. While lossless DC power flow assumptions were used for ease of presentation, our methodology applies to any linearized power flow assumptions as shown in section 3.6. For example, a linearization gap, or bias, can easily be incorporated. Marginal loss impacts can be incorporated by properly adjusting the sensitivities used, as shown in the next section. Also, it is simple to formulate hybrid TC problems, where the $B\theta$ model is used to fully describe normal operating conditions, and the shift factor model with flow-canceling transactions are used to enforce selected contingency constraints. Multi-period SCED and SCUC can be accommodated. In these problems, constraints on the maximum frequency of switching for a branch or the

³even though a max time limit of 3,600 seconds was set, some times are longer because the solver may be in the middle of an internal iteration

maximum number of switching operations in a period can be modeled.

3.4 TC Formulation with Loss Adjusted Shift Factors

While the lossless DC formulation shows promising results, most modern power markets include a linearized model of losses in their market clearing algorithm. Therefore, for Independent System Operators (ISOs) to adopt topology control, it is important to incorporate marginal losses into the TC MIP formulation. Additionally, while TC provides benefits under the DC SCOPF context it must ultimately satisfy AC OPF constraints. If the DC optimized topology is not feasible with respect to AC constraints, it is often time consuming to restore feasibility while maintaining production cost savings. Including losses in the TC MIP formulation should lead to a closer approximation of the AC OPF and thus reduce the occurrence of AC-infeasible solutions.

Resistive losses are a quadratic function of current flowing on each transmission line:

$$Loss = \sum_k I_k^2 R_k = \sum_k \frac{f_k^2 R_k}{\cos^2 \varphi_k V_k^2} \approx \sum_k \frac{f_k^2 R_k}{V_k^2}, \quad (3.41)$$

where φ_k is the angle difference between voltage and current and the approximation in the last equality depends on the assumptions that reactive power flows can be ignored (voltage and current are in phase, $\varphi_k = 0$). To incorporate a linear approximation of losses into the DC OPF we perform the standard Taylor series expansion around a base flow \mathbf{f}^0 :

$$Loss \approx \mathbf{b}^0 + \left. \frac{\partial Loss}{\partial \mathbf{f}} \right|_{\mathbf{f}^0} \mathbf{f} \quad (3.42)$$

where for a line k ,

$$\frac{\partial Loss}{\partial f_k} = \frac{2R_k}{V_k^2} f_k = x_k \quad (3.43)$$

Using (3.43) we can also express $Loss$ as

$$Loss = \frac{1}{2} \frac{\partial Loss'}{\partial \mathbf{f}} \mathbf{f} \quad (3.44)$$

Equating (3.44) and (3.42) for $\mathbf{f} = \mathbf{f}^0$ we can derive the bias term \mathbf{b}^0 as

$$\begin{aligned} Loss^0 &= \frac{1}{2} \mathbf{x}^{0'} \mathbf{f}^0 = \mathbf{b}^0 + \mathbf{x}^{0'} \mathbf{f}^0 \rightarrow \\ \mathbf{b}^0 &= -\frac{1}{2} \mathbf{x}^{0'} \mathbf{f}^0 \end{aligned}$$

Therefore, for any flow vector \mathbf{f} , we write losses as

$$Loss = \mathbf{x}^{0'} \left(\mathbf{f} - \frac{1}{2} \mathbf{f}^0 \right) \quad (3.45)$$

The term \mathbf{x}^0 is referred to as the vector of line loss factors. The loss formulation we present here is similar to one used in real markets (e.g. [26]) where losses are included in the energy balance constraint and in the flow constraints via a nodal allocation of Losses (represented below by the normalized vector \mathbf{d}). Litvinov et al. [27] showed that the advantage of this formulation compared to other approaches is that line losses and flows are reference bus independent. The formulation below is different from the one described in [27], accounting for the secondary impact of losses in equation (3.48), therefore, we will repeat the proof of reference bus independence in lemma 3.4.1. Without loss of generality, contingency constraints are excluded in the formulation below.⁴

$$\min_{\mathbf{p}} \mathbf{c}' \mathbf{p} \quad (3.46)$$

$$\text{s.t. } \mathbf{1}'(\mathbf{p} - \mathbf{l}) = Loss \quad (3.47)$$

$$Loss = \mathbf{x}^{0'} \left(\mathbf{g}^0 + \Psi(\mathbf{p} - \mathbf{l} - \mathbf{d} \cdot Loss) - \frac{1}{2} \mathbf{f}^0 \right) \quad (3.48)$$

$$\underline{\mathbf{f}} \leq \mathbf{g}^0 + \Psi(\mathbf{p} - \mathbf{l} - \mathbf{d} \cdot Loss) \leq \bar{\mathbf{f}} \quad (3.49)$$

$$\underline{\mathbf{p}} \leq \mathbf{p} \leq \bar{\mathbf{p}} \quad (3.50)$$

We will refer to constraints (3.46)-(3.49) as Formulation *L1*. In the flow constraints (3.49)

⁴Note that only losses in the base topology are included in the energy balance equation, losses in contingent topologies only impact contingent flows.

the \mathbf{d} vector allocates $Loss$ to busses. Without this term losses would be balanced at the reference bus⁵, which would imply that LMPs would also be reference bus dependent. There are many ways to select \mathbf{d} and we will not delve into this problem here. An intuitive approach, and the one we assume in this work, is to set

$$d_n = \frac{l_n}{\sum_m l_m} \quad \forall n,$$

which allocates losses to load busses in proportion to their contribution to total load.

We end this section by proving that formulation $L1$ is indeed reference bus independent and that the somewhat arbitrary choice for this bus does not impact LMPs and a large number of financial settlements.

Lemma 3.4.1. *Formulation $L1$ is reference bus independent*

Proof. To demonstrate that $L1$ is reference bus independent we modify the choice of reference bus by introducing a normalized vector \mathbf{w} that assigns a weighting to each node in proportion to its contribution to the new distributed reference bus (a single reference bus n can be represented by setting $w_n = 1$). As shown in [27], a weighting \mathbf{w} modifies the shift factor matrix according to

$$\mathbf{\Psi}_{\mathbf{w}} = \mathbf{\Psi} - \mathbf{\Psi}\mathbf{w}\mathbf{1}' \tag{3.51}$$

Substituting (3.51) into (3.48) gives

$$\begin{aligned} Loss_{\mathbf{w}} &= \mathbf{x}^{0'}(\mathbf{g}^0 + (\mathbf{\Psi} - \mathbf{\Psi}\mathbf{w}\mathbf{1}')) \cdot \\ &(\mathbf{p} - \mathbf{1} - \mathbf{d} \cdot Loss) - \frac{1}{2}f^0) = \\ \mathbf{x}^{0'}(\mathbf{g}^0 + \mathbf{\Psi}(\mathbf{p} - \mathbf{1} - \mathbf{d} \cdot Loss) - \frac{1}{2}f^0) - \\ &\mathbf{x}^{0'}\mathbf{\Psi}\mathbf{w}\mathbf{1}'(\mathbf{p} - \mathbf{1} - \mathbf{d} \cdot Loss) = Loss \end{aligned}$$

⁵since the reference bus is left out of the incidence matrix, by conservation of energy, it must absorb any imbalance

since $\mathbf{1}'(\mathbf{p} - \mathbf{l} - \mathbf{d} \cdot Loss) = 0$. Similarly, substituting (3.51) into (3.49) gives

$$\begin{aligned} \mathbf{f}_w &= \mathbf{g}^0 + (\Psi - \Psi \mathbf{w} \mathbf{1}')(\mathbf{p} - \mathbf{l} - \mathbf{d} \cdot Loss) = \\ &\quad \mathbf{g}^0 + \Psi(\mathbf{p} - \mathbf{l} - \mathbf{d} \cdot Loss) - \\ &\quad \Psi \mathbf{w} \mathbf{1}'(\mathbf{p} - \mathbf{l} - \mathbf{d} \cdot Loss) = \mathbf{f} \end{aligned}$$

We have thus shown that the constraint set is reference bus independent. Further, since the objective function is reference bus independent, by definition, the shadow prices will be reference bus independent as well. \square

3.5 TC MIP Formulation with Losses

As we saw in section 3.2.1, FCTs linearly impact flows in the same way as updating the shift factor matrix. With the introduction of losses, however, these FCTs would no longer be balanced since the injection at one end of the line is not equal to the withdrawal at the other end. In the case of losses we must redefine FCTs as the loss-adjusted canceling flows that need to be introduced so that the effect from these flows is the same as actually opening the lines⁶. Fortunately, we can still retain the same framework of the lossless shift factor TC problem. To do this, we first derive the loss-adjusted shift factor matrix, $\hat{\Psi}$ and loss-adjusted PTDF matrix, $\hat{\Phi}$, by explicitly expressing flows in terms of losses.

Re-arranging (3.48) we have

$$Loss = \frac{\mathbf{x}^{0'}(\mathbf{g}^0 + \Psi(\mathbf{p} - \mathbf{l}) - \frac{\mathbf{f}^0}{2})}{\mathbf{x}^{0'}\Psi\mathbf{d} + 1}$$

The flow equation can thus be expressed as

$$\begin{aligned} \mathbf{f} &= \mathbf{g}^0 + \Psi\left(\mathbf{p} - \mathbf{l} - \mathbf{d} \frac{\mathbf{x}^{0'}(\mathbf{g}^0 + \Psi(\mathbf{p} - \mathbf{l}) - \frac{\mathbf{f}^0}{2})}{\mathbf{x}^{0'}\Psi\mathbf{d} + 1}\right) \\ &= \mathbf{g}^0 - \Psi\mathbf{d} \frac{\mathbf{x}^{0'}(\mathbf{g}^0 - \frac{\mathbf{f}^0}{2})}{\mathbf{x}^{0'}\Psi\mathbf{d} + 1} + \Psi(\mathbf{p} - \mathbf{l}) \end{aligned}$$

⁶These FCTs will be adjusted to account for losses across all transmission lines, measured at the receiving ends.

$$\begin{aligned}
& - \Psi \mathbf{d} \frac{\mathbf{x}^{0'} \Psi (\mathbf{p} - \mathbf{l})}{\mathbf{x}^{0'} \Psi \mathbf{d} + 1} \\
& = \hat{\mathbf{g}}^0 + \Psi \left(\mathbf{I} - \frac{\mathbf{d} \mathbf{x}^{0'} \Psi}{\mathbf{x}^{0'} \Psi \mathbf{d} + 1} \right) (\mathbf{p} - \mathbf{l}) \rightarrow \\
\mathbf{f} & = \hat{\mathbf{g}}^0 + \hat{\Psi} (\mathbf{p} - \mathbf{l}) \tag{3.52}
\end{aligned}$$

from which we see that the loss-adjusted shift factor matrix and flow bias are

$$\begin{aligned}
\hat{\Psi} & = \Psi \left(\mathbf{I} - \frac{\mathbf{d} \mathbf{x}^{0'} \Psi}{\mathbf{x}^{0'} \Psi \mathbf{d} + 1} \right) \\
\hat{\mathbf{g}}^0 & = \mathbf{g}^0 - \Psi \mathbf{d} \frac{\mathbf{x}^{0'} (\mathbf{g}^0 - \frac{\mathbf{f}^0}{2})}{\mathbf{x}^{0'} \Psi \mathbf{d} + 1}
\end{aligned}$$

For completeness the flow bias \mathbf{g}^0 can be calculated as:

$$\begin{aligned}
\mathbf{g}^0 & = \mathbf{f}^0 - \Psi (\mathbf{p}^0 - \mathbf{l}^0 - \mathbf{d} \cdot \text{Loss}^0) \\
& = \mathbf{f}^0 - \Psi (\mathbf{p}^0 - \mathbf{l}^0 - \mathbf{d} \mathbf{x}^{0'} \frac{\mathbf{f}^0}{2}) \\
& = (I + \Psi \mathbf{d} \frac{\mathbf{x}^{0'}}{2}) \mathbf{f}^0 - \Psi (\mathbf{p}^0 - \mathbf{l}^0)
\end{aligned}$$

The loss-adjusted PTDF can now be expressed as:

$$\begin{aligned}
\hat{\phi}_k^\ell & = \hat{\Psi}_k^{m_\ell} - \hat{\Psi}_k^{n_\ell} \\
& = \left(\psi_k^{m_\ell} - \psi_k^{m_\ell'} \frac{\mathbf{x}^0(\psi_k \mathbf{d})}{\mathbf{x}^{0'} \Psi \mathbf{d} + 1} \right) \\
& \quad - \left(\psi_k^{n_\ell} - \psi_k^{n_\ell'} \frac{\mathbf{x}^0(\psi_k \mathbf{d})}{\mathbf{x}^{0'} \Psi \mathbf{d} + 1} \right) \\
& = \phi_k^\ell - \phi_k^{k'} \mathbf{x}^0 \frac{\psi_k \mathbf{d}}{\mathbf{x}^{0'} \Psi \mathbf{d} + 1}
\end{aligned}$$

where ψ^{m_ℓ} denotes the column of Ψ corresponding to bus m and ϕ^k denotes the column of Φ corresponding to line k . Although this derivation is not necessary for the MIP formulation it provides some intuition for how the PTDF is adjusted for losses. We should note that although the loss-adjusted shift factors and PTDF matrices depend on an initial

dispatch and set of flows, they can nevertheless be pre-calculated from the original shift factor matrix using only matrix multiplication, which would be fast even for large systems. With these loss-adjusted shift factors and PTDFs we can now express loss-adjusted FCTs similarly to (3.17). In addition, since the $Loss$ equation is a function of flows, we can apply FCTs to update $Loss$ for line openings. Partitioning transmission losses into losses from monitored and switchable lines respectively, we have:

$$\begin{aligned} Loss^{\mathcal{M}} &= \mathbf{x}^{0'} (\hat{\mathbf{g}}^{0\mathcal{M}} - \frac{1}{2} \mathbf{f}^{0\mathcal{M}} + \hat{\Psi}_{\tau_0}^{\mathcal{M}} (\mathbf{p} - \mathbf{1}) + \hat{\Phi}_{\tau_0}^{\mathcal{M}\mathcal{S}} \mathbf{v}_{\tau_0}) \\ Loss^{\mathcal{S}} &= \mathbf{x}^{0'} (\hat{\mathbf{g}}^{0\mathcal{S}} - \frac{1}{2} \mathbf{f}^{0\mathcal{S}} + \hat{\Psi}_{\tau_0}^{\mathcal{S}} (\mathbf{p} - \mathbf{1}) + (I - \hat{\Phi}_{\tau_0}^{\mathcal{S}\mathcal{S}}) \mathbf{v}_{\tau_0}) \end{aligned}$$

Finally, the full topology control DC SCOPF MIP with losses is:

$$\mathcal{C} = \min_{\mathbf{p}, \mathbf{v}, \mathbf{z}} \mathbf{c}' \mathbf{p} \quad (3.53)$$

$$\text{s.t. } \mathbf{1}' (\mathbf{p} - \mathbf{1}) - Loss = 0 \quad (3.54)$$

$$Loss = Loss^{\mathcal{M}} + Loss^{\mathcal{S}} \quad (3.55)$$

$$Loss^{\mathcal{M}} = \mathbf{x}^{0\mathcal{M}'} (\hat{\mathbf{g}}^{0\mathcal{M}} - \frac{1}{2} \mathbf{f}^{0\mathcal{M}} + \hat{\Psi}_{\tau_0}^{\mathcal{M}} (\mathbf{p} - \mathbf{1}) + \hat{\Phi}_{\tau_0}^{\mathcal{M}\mathcal{S}} \mathbf{v}_{\tau_0}) \quad (3.56)$$

$$Loss^{\mathcal{S}} = \mathbf{x}^{0\mathcal{S}'} (\hat{\mathbf{g}}^{0\mathcal{S}} - \frac{1}{2} \mathbf{f}^{0\mathcal{S}} + \hat{\Psi}_{\tau_0}^{\mathcal{S}} (\mathbf{p} - \mathbf{1}) + (\hat{\Phi}_{\tau_0}^{\mathcal{S}\mathcal{S}} - \mathbf{I}) \mathbf{v}_{\tau_0}) \quad (3.57)$$

$$\underline{\mathbf{f}}_{\tau}^{\mathcal{M}} \leq \hat{\mathbf{g}}_{\tau}^0 + \hat{\Psi}_{\tau}^{\mathcal{M}} (\mathbf{p} - \mathbf{1}) + \hat{\Phi}_{\tau}^{\mathcal{M}\mathcal{S}} \mathbf{v}_{\tau} \leq \bar{\mathbf{f}}_{\tau}^{\mathcal{M}}, \quad \forall \tau \quad (3.58)$$

$$\underline{\mathbf{f}}_{\tau}^{\mathcal{S}} \mathbf{z} \leq \hat{\mathbf{g}}_{\tau}^0 + \hat{\Psi}_{\tau}^{\mathcal{S}} (\mathbf{p} - \mathbf{1}) + (\hat{\Phi}_{\tau}^{\mathcal{S}\mathcal{S}} - \mathbf{I}) \mathbf{v}_{\tau} \leq \bar{\mathbf{f}}_{\tau}^{\mathcal{S}} \mathbf{z}, \quad \forall \tau \quad (3.59)$$

$$-M (\mathbf{1} - \mathbf{z}) \leq \mathbf{v}_{\tau} \leq M (\mathbf{1} - \mathbf{z}), \quad \forall \tau \quad (3.60)$$

$$\underline{\mathbf{p}} \leq \mathbf{p} \leq \bar{\mathbf{p}} \quad (3.61)$$

$$z_{\ell} \in \{0, 1\}, \quad \forall \ell \in \mathcal{S} \quad (3.62)$$

We refer to problem (3.53)-(3.62) as the *Loss-adjusted shift factor TC formulation*. Note that the $\mathbf{d} \cdot Loss$ term in the above formulation is replaced via the equivalence relationship shown in (3.52). Generally, ISOs may only monitor a subset of all transmission lines for losses. This means that $Loss$ will be aggregated over a set that is smaller than $\mathcal{M} \cup \mathcal{S}$.

In the extreme case when no lines in \mathcal{S} are monitored for losses, constraint (3.57) would be empty. If additionally the end nodes of lines in \mathcal{S} are not load busses ($d_m, d_n = 0$), constraints (3.59) would reduce to (3.26) and FCTs would be calculated independent of losses as in the *Shift factor TC formulation*

3.5.1 LMPs and Loss-Adjusted Formulation

In this section we derive LMPs under the loss-adjusted shift factor TC formulation and prove that opening branches may be beneficial for reducing losses, even with no congestion. While there have been case studies and experimental results showing the impact of topology control on losses [7,8], in this section we derive an explicit relationship between the marginal benefit of branch switching and the impact on system losses.

Similarly to the derivation in section 3.2.3 we take the derivative of the Lagrangian with respect to demand (substituting the loss equation directly into the energy balance constraint to avoid introducing additional shadow prices)

$$\begin{aligned}
LMP &= \lambda \mathbf{1} - \lambda (\hat{\Psi}_{\tau_0}^{\mathcal{M}'} \mathbf{x}^{0^{\mathcal{M}}} + \hat{\Psi}_{\tau_0}^{\mathcal{S}'} \mathbf{x}^{0^{\mathcal{S}}}) \\
&- \hat{\Psi}^{\mathcal{M}'}(\bar{\underline{\mu}} - \underline{\mu}) - \hat{\Psi}^{\mathcal{S}'}(\bar{\underline{\alpha}} - \underline{\alpha}) = \\
&= \lambda \mathbf{1} - \lambda \hat{\Psi}'_{\tau_0} \mathbf{x}^0 \\
&- \hat{\Psi}^{\mathcal{M}'}(\bar{\underline{\mu}} - \underline{\mu}) - \hat{\Psi}^{\mathcal{S}'}(\bar{\underline{\alpha}} - \underline{\alpha})
\end{aligned} \tag{3.63}$$

Performing the same substitutions as in section 3.2.3 we see that the LMP derived from the loss-adjusted TC MIP formulation is

$$\begin{aligned}
LMP &= \lambda \mathbf{1} - \lambda \left(\hat{\Psi}_{\tau_0}^{\mathcal{M}'} + \hat{\Psi}_{\tau_0}^{\mathcal{S}'} \hat{\mathbf{O}}_{\tau_0}^{\mathcal{M}\mathcal{S}'} \right) \mathbf{x}^{0^{\mathcal{M}}} \\
&- \left(\hat{\Psi}^{\mathcal{M}'} + \hat{\Psi}^{\mathcal{S}'} \hat{\mathbf{O}}^{\mathcal{M}\mathcal{S}'} \right) (\bar{\underline{\mu}} - \underline{\mu})
\end{aligned} \tag{3.64}$$

We observe that equation (3.35) has a loss component, which is only relevant in topology τ_0 .

By appropriately grouping terms by topology we can partition (3.35) into two components:

$$\begin{aligned} (\bar{\alpha}_{\tau_0} - \underline{\alpha}_{\tau_0}) &= \hat{\mathbf{O}}_{\tau_0}^{\mathcal{MS}'}(\bar{\boldsymbol{\mu}}_{\tau_0} - \underline{\boldsymbol{\mu}}_{\tau_0}) \\ &+ \lambda \left(\hat{\mathbf{O}}_{\tau_0}^{\mathcal{MS}'} \mathbf{x}^{0^{\mathcal{M}}} - \mathbf{x}^{0^{\mathcal{S}}} \right) \end{aligned} \quad (3.65)$$

and

$$(\bar{\alpha}_{\tau} - \underline{\alpha}_{\tau}) = \hat{\mathbf{O}}_{\tau}^{\mathcal{MS}'}(\bar{\boldsymbol{\mu}}_{\tau} - \underline{\boldsymbol{\mu}}_{\tau}) \quad \forall \tau \neq \tau_0 \quad (3.66)$$

Expressions (3.65)-(3.66) are similar to the relationship between shadow prices for switchable and monitored lines reported in section 3.2.3. This relationship provides a generalization of the "total derivative" concept for line openings introduced in that section, where $\bar{\alpha}_{\tau} - \underline{\alpha}_{\tau}$ reflects the marginal value (positive or negative) of line switching. As shown in (3.65), this value consists of both congestion and loss components. The congestion component is the scalar product of shadow prices for monitored constraints and LODFs of the open line on these constraints. The loss component is the difference between: the impact of line opening on losses in monitored facilities (LODFs multiplied by the corresponding line loss factors) and, the loss factors of open lines.

If we assume for a moment that there is no congestion in the system, equation (3.65) is very intuitive, saying that opening a branch is beneficial (in the marginal sense) if the reduction in losses due to removing that branch offsets the increase in losses on all monitored branches. While in the lossless formulation branch opening is never beneficial in the absence of transmission congestion (congestion component equals zero), incorporating marginal losses recognizes potential benefits of topology control due to a reduction in losses, which may be realized in the absence of congestion.

In the next section we present some results of modeling with loss-adjusted shift factors and compare them to the lossless formulation

3.5.2 Loss-Adjusted TC Simulations on the IEEE 118-bus System

To study the impact of losses in the shift factor formulation we used the publically available IEEE 118-bus test system. We fixed a set of 16 switchable lines (selected using some of the policies detailed in [17]) and performed a Monte Carlo over 100 samples using the approach described in section 3.3. For each sample we modeled the lossless DC SCOPF and the DC SCOPF with shift factors and bias terms adjusted for losses⁷. Taking the optimal topology from each of the two formulations we verified the solution against the full set of AC power flow equations for each sample to assess the feasibility of the DC solutions and the (p.u.) congestion cost savings. Per-unit (p.u.) congestion savings are calculated as

$$\%Savings = \frac{C_{MIP} - C_{base}}{C_{base} - C_0} \quad (3.67)$$

where C_{MIP} is the system cost from the DC MIP or from the AC OPF based on this MIP, C_{base} is the DC or AC system costs with no switching and C_0 is the DC or AC system cost with no enforced transmission constraints. $C_{base} - C_0$ represents the maximum savings possible for any sample. Congestion cost savings for the DC and AC models are calculated relative to the DC and AC models with no TC respectively. Table 3.4 below summarizes the results from which we make three key observations. First, based on the

Table 3.4: Median Number of Line Openings and Average Per-unit Congestion Costs Savings with different loss modeling assumptions over 100 Samples

Model	Num. Lines Opened	Congestion Cost Savings with TC
DC w/Losses	11	16.64%
DC Lossless	14	22.09%
AC Based on DC w/Losses	N/A	20.66%
AC Based on DC Lossless	N/A	20.65%

AC SCOPF solutions, accounting for losses does not improve congestion cost savings. The AC OPF based on the loss-adjusted DC MIP solution produces more savings in 53 of the

⁷In the lossless formulation the bias term is calculated as $\mathbf{g}^0 = \mathbf{f}^0 - \Psi(\mathbf{p}^0 - \mathbf{1}^0)$.

samples, compared to the AC OPF based on the lossless DC MIP, however, the magnitude in savings tends to be greater for the latter model so that both AC solutions lead to about the same 20.65% p.u. congestion cost savings. Second, solving the AC SCOPF using the optimal topologies from the two DC formulations confirms that both DC formulations reflect legitimate congestion cost savings. The lossless MIP formulation overstates the benefits from switching by an average of 1.44% in 76 samples while the loss-adjusted MIP understates them by 4.03% in 93 samples. Both formulation, however, provide a good indication of potential savings from topology control. Finally, we observe that the loss-adjusted DC MIP tends to open 3 fewer lines than its lossless counterpart. Opening fewer lines is clearly preferable; operating circuit breakers, although not included explicitly in these simulations, has a cost and, achieving the same savings with fewer openings is more efficient and reduces the number of discrete changes to the state of the system. Figure 3.2 below shows the number of line openings across all samples. As shown in the figure,

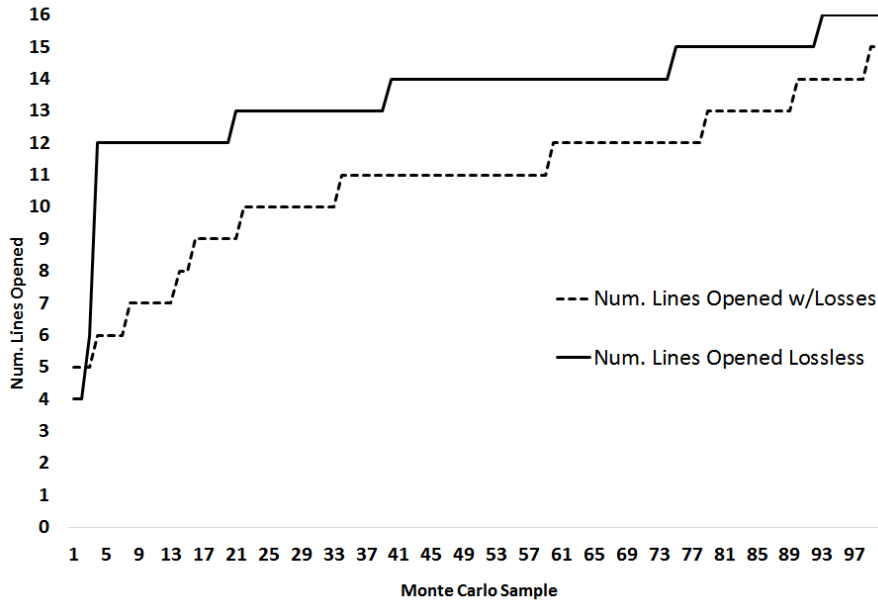


Figure 3.2: Number of Lines Opened in DC MIP Formulations

the loss-adjusted MIP opens between 1 and 9 fewer lines in 79 samples, opens the same

number of lines in 18 samples, and opens only 1 additional line in 3 samples.

3.6 TC Formulation with AC Modeling

One application of topology control is for real-time markets. Real-time markets tend to be cleared every five minutes with a 5 to 15 minute look ahead. The market clearing algorithms rely on a linearized AC model with shift factors and other parameters updated using state estimator data. To integrate topology control algorithms into the existing market process, the maximum admissible solution time is 5 minutes, which could make iterating between the DC and AC models impractical in large systems such as PJM. In this section we report on the performance of algorithms similar to those previously proposed [17, 25], where AC rather than DC power flow equations are used. Unlike the DC-based algorithm results, the AC-based algorithms do not rely on an approximate system state representation. AC-based algorithms model both real and reactive power flows, losses and bus voltage magnitudes and angles, and rely on linearization to achieve the requisite computational speed in the optimization problem. In the context of real-time markets, each solution must be provided by the topology control process within five minutes. The evidence reported here re-affirms that topology control algorithms (TCA) can reduce congestion costs and provide novel congestion control options. In addition, it shows that TCA can be implemented in a control room environment that requires computational performance as well as AC power flow accuracy, which we henceforth refer to as AC-feasibility.

The dataset used for AC modeling is more complete compared to the one described in section 3.3. Due to limitations of the $B\theta$ formulation, a number of constraints were removed from the dataset in 3.3 to be able to compare simulation results (those constraints are included in the results of the next section). In collaboration with PJM, three representative weeks from the summer, winter and shoulder seasons were selected as a basis for estimating annual savings. The DC as well as AC-based TC models employed in this section were formulated to accept the same dataset as the one employed in the actual PJM real-time

market. We note below the basic dataset characteristics:

- 13,000+ buses (consolidated bus-branch models)
- 500 dispatchable thermal generation units
- 20,000 branches (3,500 monitored branches)
- 6,000 single and multi-element contingencies

The dataset includes power flows from the PJM state estimator, monitored transmission and contingency constraints, and economic generation and transmission data from the real-time markets. These data were used to create TCA inputs for each of the 168 hours in each representative week.

The DC-based model results that we presented in 3.3 relied on the following simplifying assumptions:

- Power flow equations are limited to real power only and bus voltage magnitudes are assumed to be at 1.0 per unit
- Losses are taken from the state estimator AC case and distributed among the loads. The distributions and loss magnitude are not adjusted with topology or dispatch changes
- Contingency analysis relies on the DC power flow approximation and ignores changes in reactive flows

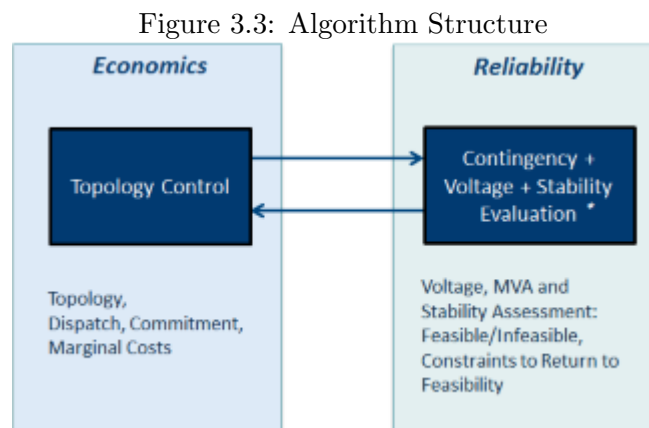
In this section we modify our previous TCA formulation to incorporate AC power flow modeling. The OPF is solved using a linearized AC power flow formulation (see for example [13]) and contingency analysis also account for reactive flows. In contrast to the DC model, the AC TCA formulation represents both real and reactive power flows as well as voltage magnitudes and angles at buses. Losses are calculated from the AC power flow solution and automatically updated at each TCA iteration. Compared to the DC model in section 3.2.2,

the AC formulation guarantees AC feasibility at every step of the TCA, with sustainable impact on computation performance.

The iterative TCA formulation is summarized in the following 4 steps:

- Using heuristics in [17, 25] identify switchable line candidates for TC action. If good candidates are identified, proceed to the next step, otherwise skip to the last step
- Evaluate the benefits of switching the selected candidates on an AC model
- Evaluate flows of monitored facilities for all contingencies to verify that the post-switch-action topology is N-1 secure. The switching action is reverted if the security criterion is not met.
- Repeat the previous steps until a stopping criterion is reached.
- Specify the associated topology as final for the interval and proceed to the next interval (hourly intervals are used in the simulations).

Figure 3.3 depicts the steps above



At each step in the Reliability assessment, all 3,500 branches are monitored in the contingency analysis. This is a comprehensive list of facilities that do not need to change

with topology.⁸ With the exception of transient and voltage stability, which are not assessed in this work, this algorithm ensures AC feasibility at each iteration described above.⁹ By solving the AC power flow we accurately capture losses as the topology changes and include these losses explicitly in the formulation employed by the TCA heuristics. Leveraging parallel computing options in performing the above steps, the proposed solution for each hour requires less than five minutes (it aligns with the five minute real-time market at PJM), and as shown in the next section performs similarly to the DC model in terms of line openings and congestion cost savings.

3.6.1 AC Modeling Results for the PJM System

Based on computational results from the three representative weeks of 2010, the estimated annual savings in the PJM real-time market under 2010 conditions are estimated to be over \$100 million. Table 3.5 reports detailed weekly savings. The term *Cost of Conges-*

Table 3.5: Summary of Savings achieved by TCA (millions of dollars)

Week	Cost of Congestion	Savings From TCA	% Savings Captured
2010 Summer	\$6.7	\$2.9	44%
2010 Winter	\$4.2	\$2.8	68%
2010 Shoulder	\$1.6	\$1.1	67%

tion represents the additional production cost that results from the generation re-dispatch required to avoid transmission line capacity violations, and, as such, it is the maximum conceivable savings that TC can achieve. More precisely, *Cost of Congestion* is defined as the difference between generation production costs with the historical topology and enforced transmission constraints and the production costs in the absence of transmission constraints.

⁸While there are 20,000 lines total, they include lines outside of PJM, lines connected in series, generation step up transformers, lower voltage facilities and other branches that are typically not explicitly monitored

⁹The inclusion of stability evaluations is not expected to significantly reduce the potential TCA savings, given preliminary analyses and considering PJM system characteristics and the nature of usual system limitations.

Figures 3.4-3.6 compare the results above to savings found under the DC-based algorithms. The total cost of congestion estimated by the AC power flow model is smaller, primarily, due to the incorporation of marginal losses that were ignored in the DC model. The lossless transfer of power across large distances as modeled in the DC-OPF model underestimates costs and hence overestimates savings from dispatching distant low-cost generation. Since the cost of congestion in the DC OPF is estimated to be higher relative to the linearized AC OPF, total savings are evaluated to be lower by the AC power flow model. The relative cost of congestion savings, however, are similar. Moreover, the AC-based TCA switching solution is AC feasible, whereas the DC solution need not be.

Figure 3.4: Cost of Congestion

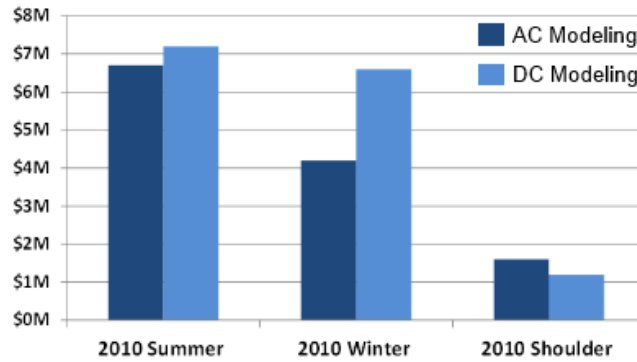
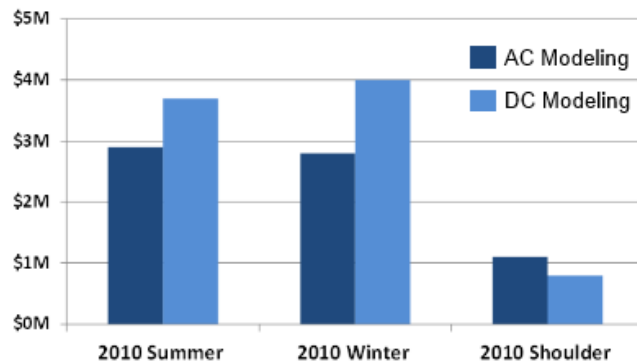
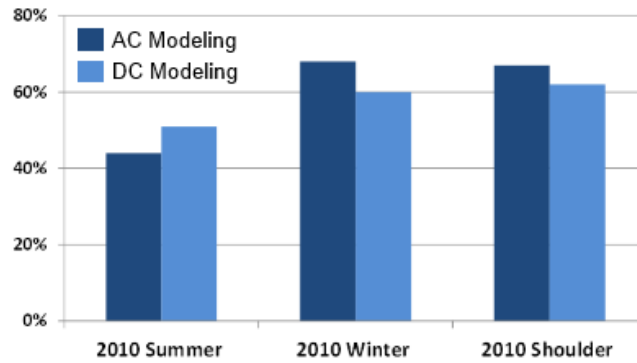


Figure 3.5: Savings



Figures 3.7-3.9 compare the number of lines opened in the three 2010 weeks. The ramp-up trend in the first 24 hours of each figure is due to the incremental nature of the algorithm

Figure 3.6: % Savings Captured



where each consecutive hour begins by inheriting the optimized topology of the previous hour. Since the first hour of the week does not inherit any opened lines, we observe that it takes about 24 hours for the number of lines opened to reach their “average” level. As

Figure 3.7: Branches Open with TCA - 2010 Summer

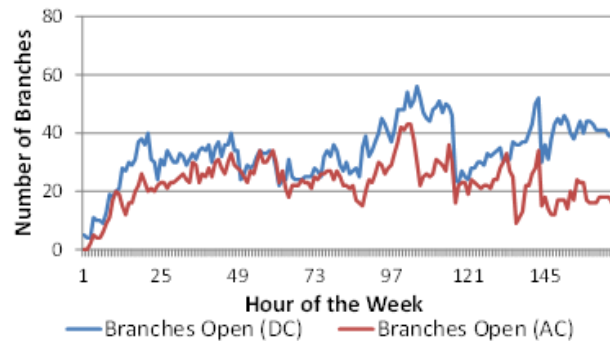


Figure 3.8: Branches Open with TCA - 2010 Winter

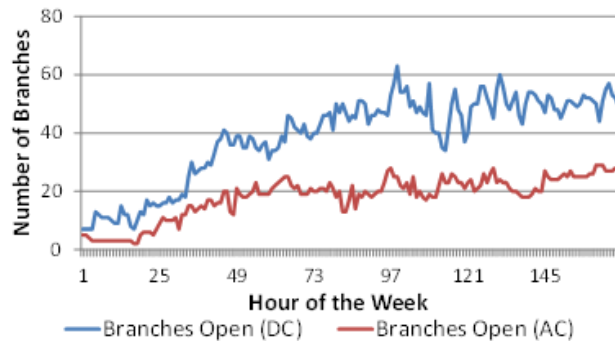
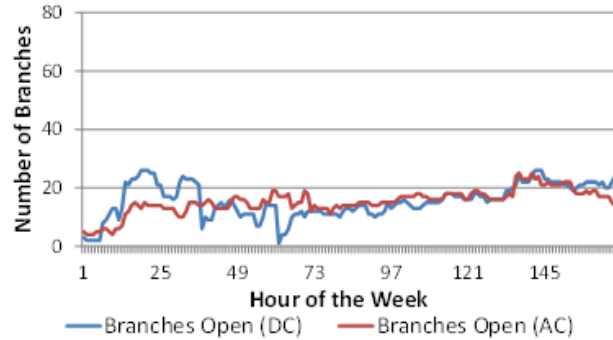


Figure 3.9: Branches Open with TCA - 2010 Shoulder



shown in the figures, fewer lines are opened by the AC-based TCA during the higher load weeks (summer and winter). The main reason for this difference is the explicit modeling of marginal losses. Marginal losses increase as the system flows increase, which tends to happen under higher load conditions. With marginal loss modeling, the incremental cost savings of opening a branch has to be larger than the potential increments in costs due to losses increase. Lines associated with a high congestion-relieving marginal benefit in the lossless formulation may have an adverse impact on system losses. Thus, fewer branches are beneficial for opening under AC modeling. It is interesting to note that a similar effect was observed when we included losses in the DC-based TCA. As shown in figure 3.6, the relative savings achieved by TCA are similar with and without loss modeling. In addition, opening fewer lines is clearly beneficial from an operations point of view. We also note that the AC-based TCA opens fewer lines than the DC-based TCA with loss modeling. This indicates that the AC-based TCA is usually constrained by the 5 minute computing time limit and analyzed fewer candidates.

Table 3.6 summarizes the frequency of branches switched open by the algorithm, classified by their nominal voltage level. In all three weeks, 56-59% of lines opened do not exceed 230 kV while 70% of all lines opened do not exceed 345 kV. Compared to the DC-based TCA results, in which over 80% of lines opened did not exceed 345 kV, the AC-based TCA opens a fewer percentage of low-voltage lines. Incorporating losses and reactive power

Table 3.6: Summary of Line Switchings by Voltage Level

Nominal kV	<200 kV	230 kV	345 kV	500 kV	765 kV
2010 Summer	35%	21%	14%	22%	8%
2010 Winter	36%	21%	20%	12%	10%
2010 Shoulder	16%	43%	14%	17%	10%

appears to make it less desirable to open low-voltage lines.

The general behavior of the branches switched are that lower voltage lines tend to stay open for longer strings of hours while higher voltage lines typically stay open for shorter periods. For branches below 230 kV, they make up 56-69% of the number of switching operations, but 67-75% of the hours in which branches are open. Conversely, at the 765 kV level, they represent 8-10% of the number of switching operations, but only 3-7% of the total number of hours in which branches are open. Higher voltage lines are generally opened over shorter periods that are associated with light load conditions.

Table 3.7 compares AC-based and DC-based TCA results in terms of some additional opening and closing statistics during the summer week. Again, we consistently observe

Table 3.7: Topology Change Statistics Summary - Summer Week

	AC DC	AC DC	AC DC
	Branches	Switched	Switched
percentile	Open	Open	Close
Min	0 4	0 0	0 0
25%	18 28	0 1	1 1
Median	23 33	2 3	2 2
75%	27 40	4 5	3 4
Max	43 56	10 10	23 29

fewer lines opened by the AC-based TCA with the median number of lines open at any given time trailing that of the DC-based TCA by about 10. In any given hour, however, both models open a small number of lines, with only one or two additional lines opened by the DC-based TCA. The winter week exhibits the same behavior as the summer week while the statistics for the shoulder week are almost identical among the AC and DC-based models (as shown in figure 3.9). In the shoulder season demand is lower, marginal

losses have less impact, and the time constraint of five minutes is often not limiting the evaluation of promising switchable line candidates. Consequently, results between the AC and DC-based models are quite similar.

This section demonstrates the applicability of TCA to real systems in a control room environment. By incorporating AC power flow modeling, we ensure AC feasible at every step of the TCA. In addition, we can accurately model branch MVA limits, and the inclusion of losses makes the TCA solutions more realistic. Compared to DC-based TCA, the AC-based formulation is computationally more expensive. As a result, the AC-based TC algorithm tends to evaluate fewer candidate lines within the imposed five minute time constraint. Nevertheless, the results above show that the relative savings captured by the AC-based TCA is substantial. In addition, the AC-based TCA opens fewer lines, which is more attractive to system operators and transmission owners from an implementation perspective. The evidence reported on the tractability of DC-based TCA in reducing congestion costs on a system the size of PJM is replicated here for the AC-based TCA, which additionally ensures the AC feasibility required for operational TC actions. In conclusion, there is strong evidence to support the ability of TCA to be usefully employed in operations.

Chapter 4

Substation Reconfiguration

Substation reconfiguration is an additional TC action, which consists of opening or closing breakers that are not in series with branches or transformers. Some substation reconfiguration actions are simpler to implement from an operations point of view than branch opening, seen as a less invasive action in which fewer switching devices are operated. In this chapter we introduce two formulations that incorporate substation reconfiguration with branch opening in a unified TC framework. We provide a theoretical framework for both methods and formulate security-constrained shift factor MIP TC formulations that incorporate both breaker and branch switching. By maintaining the shift factor formulation we take advantage of its compactness, especially in the context of contingency constraints, and by focusing on reconfiguring substations we hope to provide system operators additional flexibility in their TC decision processes.

The substation reconfiguration problem has been studied [4, 28–30] in the context of corrective switching, overload/voltage relief and congestion cost savings. In [30] the authors describe a ranking-based, iterative algorithm for both branch and breaker switching and apply it to the Public Service Electric & Gas Co. In [28] the authors employ a $B\theta$ formulation of power flows to model breaker opening and in [4, 29] the authors describe a voltage distribution factor-based model for topology control that considers both real and reactive power, however, breakers are approximated as having a very small impedance. These approximations are prone to errors and numerical issues due to ill-conditioning of matrices when the range in magnitude between the smallest and largest coefficient is too large as would be the case when assuming a very small impedance for a breaker. This

chapter derives a shift factor framework for explicitly modeling breakers in power flow equations and introduces two TC MIP formulations to optimize substation configuration in the SCOPF problem. By formulating the TC problem in the shift factor framework we expect to achieve faster solution times (especially with contingency constraints) and to be more consistent with the type of models being solved in ISO markets.

The first TC MIP formulation presented in this chapter can be thought of as the reverse of the FCT formulation used in branch switching. It starts with a topology where all candidate breakers are open and introduces breaker closing transactions (BCT) to simulate the closing of breakers (in contrast to FCTs, which model opening of non-zero-impedance branches). The second formulation starts from a network topology with all candidate breakers closed and introduces breaker opening incremental flows (BOIFs) that simulate the opening of breakers. The state of the topology, the number of candidate substations and the system operators objectives will dictate the choice of formulation.

4.1 MIP Formulation with BCTs

In chapter 2 we derived a shift factor based OPF formulation for modeling zero-impedance breakers. In order to formulate a MIP with BCTs we need to find the impact of closing breakers on the rest of the system and the magnitude of the BCT when a breaker is closed. This impact of breaker closing on monitored branches is the branch closing distribution factor (LCDF) and is defined by $\frac{d\mathbf{f}_\tau^{\mathcal{N}}}{d\mathbf{f}_\tau^{\mathcal{Z}}}$. Differentiating equations (2.43) - (2.45) with respect to $\mathbf{f}_\tau^{\mathcal{Z}}$ (see chapter 2), we have

$$\frac{d\mathbf{f}_\tau^{\mathcal{N}}}{d\mathbf{f}_\tau^{\mathcal{Z}}} = \frac{d\theta_\tau}{d\mathbf{f}_\tau^{\mathcal{Z}}} \mathbf{A}_\tau^{\mathcal{N}'} \tilde{\mathbf{B}}_\tau^{\mathcal{N}} \quad (4.1)$$

$$\frac{d\theta_\tau}{d\mathbf{f}_\tau^{\mathcal{Z}}} \mathbf{A}_\tau^{\mathcal{Z}'} = 0 \quad (4.2)$$

$$\frac{d\mathbf{f}_\tau^{\mathcal{N}}}{d\mathbf{f}_\tau^{\mathcal{Z}}} \mathbf{A}_\tau^{\mathcal{N}} + \mathbf{A}_\tau^{\mathcal{Z}} = 0 \quad (4.3)$$

Repeating a similar set of algebraic manipulations as for the shift factor calculation in chapter 2, we arrive at

$$\begin{aligned} \left(\frac{d\mathbf{f}_\tau^{\mathcal{N}}}{d\mathbf{f}_\tau^{\mathcal{Z}}}\right)' &= -\tilde{\mathbf{B}}_\tau^{\mathcal{N}} \mathbf{A}_\tau^{\mathcal{N}} \left(\mathbf{A}_\tau^{\mathcal{N}'} \tilde{\mathbf{B}}_\tau^{\mathcal{N}} \mathbf{A}_\tau^{\mathcal{N}}\right)^{-1} \mathbf{A}_\tau^{\mathcal{Z}'} \\ &= (\hat{\Psi}_\tau) \mathbf{A}_\tau^{\mathcal{Z}'} = (\hat{\Phi}_\tau^{\mathcal{N}\mathcal{Z}}) \end{aligned} \quad (4.4)$$

where $\hat{\Psi}$ and $\hat{\Phi}$ refer to the topology with candidate breakers opened. The LCDF in (4.4) can be used to emulate the closing of a breaker by an injection and withdrawal at its terminals.

To determine the magnitude of the breaker closing transactions when $z_\ell = 1$ we can take two approaches. From the shift factors derived in chapter 2, the flow on closed breakers is

$$\begin{aligned} \mathbf{f}_\tau^{\mathcal{Z}} &= \Psi_\tau^{\mathcal{Z}}(\mathbf{p} - \mathbf{1}) \\ &= -\left(\mathbf{A}_\tau^{\mathcal{Z}} \mathbf{B}_\tau^{-1} \mathbf{A}_\tau^{\mathcal{Z}'}\right)^{-1} \mathbf{A}_\tau^{\mathcal{Z}} \mathbf{B}_\tau^{-1}(\mathbf{p} - \mathbf{1}) \end{aligned} \quad (4.5)$$

from which we can write

$$\left(\mathbf{A}_\tau^{\mathcal{Z}} \mathbf{B}_\tau^{-1} \mathbf{A}_\tau^{\mathcal{Z}'}\right) \mathbf{f}_\tau^{\mathcal{Z}} + \mathbf{A}_\tau^{\mathcal{Z}} \mathbf{B}_\tau^{-1}(\mathbf{p} - \mathbf{1}) = 0 \quad (4.6)$$

Alternatively, from the $B\theta$ formulation, we know that the angle difference across breakers is 0. When $z = 1$, we impose this requirement in the shift factor formulation by appropriately setting the decision variable \mathbf{p} . By applying equation (2.47) we have

$$\mathbf{A}_\tau^{\mathcal{Z}} \frac{d\theta_\tau'}{d\mathbf{p}}(\mathbf{p} - \mathbf{1}) = 0 \quad (4.7)$$

Expanding out the terms using (2.50), we have

$$\begin{aligned} -\mathbf{A}_\tau^{\mathcal{Z}} \mathbf{B}_\tau^{-1}(\mathbf{I} + \mathbf{A}_\tau^{\mathcal{Z}'} \Psi_\tau^{\mathcal{Z}})(\mathbf{p} - \mathbf{1}) &= \\ \mathbf{A}_\tau^{\mathcal{Z}} \mathbf{B}_\tau^{-1}(\mathbf{p} - \mathbf{1}) + \mathbf{A}_\tau^{\mathcal{Z}} \mathbf{B}_\tau^{-1} \mathbf{A}_\tau^{\mathcal{Z}'} \mathbf{v}_\tau^{\mathcal{Z}} &= 0 \end{aligned} \quad (4.8)$$

Equations (4.6) and (4.8) are identical, where the BCT, \mathbf{v}_τ^z is precisely the flow on closed breakers given by

$$\mathbf{v}_\tau^z = \Psi_\tau^z(\mathbf{p} - \mathbf{l}) \quad (4.9)$$

Using (4.8) we can now formulate the MIP as follows

$$\mathcal{C} = \min_{\mathbf{p}, \mathbf{v}, \mathbf{t}} \mathbf{c}'\mathbf{p} \quad (4.10)$$

$$\text{s.t. } \mathbf{1}'(\mathbf{p} - \mathbf{l}) = 0 \quad (4.11)$$

$$\underline{\mathbf{p}} \leq \mathbf{p} \leq \bar{\mathbf{p}} \quad (4.12)$$

$$\underline{\mathbf{f}}_\tau^M \leq \mathbf{g}_\tau^0 + \hat{\Psi}_\tau^M(\mathbf{p} - \mathbf{l}) - \hat{\Phi}_\tau^{Mz} \mathbf{v}_\tau^z \leq \bar{\mathbf{f}}_\tau^M \quad \forall \tau \quad (4.13)$$

$$-M(\mathbf{1} - \mathbf{t}^z) \leq \left(\mathbf{A}_\tau^z \mathbf{B}_\tau^{-1} \mathbf{A}_\tau^{z'} \right) \mathbf{v}_\tau^z +$$

$$\mathbf{A}_\tau^z \mathbf{B}_\tau^{-1}(\mathbf{p} - \mathbf{l}) \leq M(\mathbf{1} - \mathbf{t}^z) \quad \forall \tau \quad (4.14)$$

$$-M\mathbf{t}^z \leq \mathbf{v}_\tau \leq M\mathbf{t}^z \quad \forall \tau \quad (4.15)$$

$$\mathbf{t}^z \in \{0, 1\} \quad (4.16)$$

Equations (4.10) - (4.13) are identical in structure to the branch switching formulation¹. Specifically, equation (4.13) enforces the flows on monitored branches, which are impacted by all breaker closing transactions. Equations (4.14) and (4.15) force the flow on breakers to (4.5) when $z = 1$ and otherwise leave equation (4.14) unconstrained. One complication in this formulation is that equations (4.13) and (4.14) rely on calculating \mathbf{B}^{-1} for every contingent topology τ . However, using Woodbury's matrix inversion lemma, we can update \mathbf{B}^{-1} very efficiently and avoid many large matrix inversions. In the special case where a contingent topology has only one outaged branch, ℓ , the update is of the following form

$$\mathbf{B}_\tau^{-1} = \left(\mathbf{B}_0^{-1} - \frac{1}{b_\ell} \mathbf{u}\mathbf{u}' \right)^{-1} \quad (4.17)$$

¹The only difference is the sign on the PTDF matrix in (4.13). This is because we are simulating branch closing distribution factors as opposed to branch opening distribution factors

which can be computed quickly using the matrix inversion lemma.

4.1.1 MIP Formulation with BCTs and FCTs

For completeness this section combines breaker closing with branch opening to formulate a joint formulation. Including flow-cancelling transactions requires a few small changes. We first need to introduce \mathbf{v}_τ^S and \mathbf{t}^S to represent flow-cancelling transactions and the binary branch switching variables. Constraints (4.15) would be introduced for FCTs and the term $\hat{\Phi}_\tau^{MS} \mathbf{v}_\tau^S$ would be added to equations (4.13). Equation (4.14) would change since the flow on breakers would now be impacted by FCTs:

$$\begin{aligned} \mathbf{f}_\tau^Z &= -\left(\mathbf{A}_\tau^Z \mathbf{B}_\tau^{-1} \mathbf{A}_\tau^{Z'}\right)^{-1} \mathbf{A}_\tau^Z \mathbf{B}_\tau^{-1} (\mathbf{p} - \mathbf{l}) + \\ &\hat{\Phi}_\tau^{ZS} \mathbf{v}_\tau^S \end{aligned} \quad (4.18)$$

By multiplying both sides by the invertible matrix on the right hand side and collecting terms we arrive at

$$\mathbf{A}_\tau^Z \mathbf{B}_\tau^{-1} \left(\mathbf{A}_\tau^{Z'} \mathbf{f}_\tau^Z + (\mathbf{p} - \mathbf{l}) - \mathbf{A}_\tau^{Z'} \hat{\Phi}_\tau^{MS} \mathbf{v}_\tau^S \right) = 0 \quad (4.19)$$

Equations (4.20)-(4.28) define the MIP formulation with both forms of topology control actions:

$$\mathcal{C} = \min_{\mathbf{p}, \mathbf{v}, \mathbf{t}} \mathbf{c}' \mathbf{p} \quad (4.20)$$

$$\text{s.t. } \mathbf{1}' (\mathbf{p} - \mathbf{l}) = 0 \quad (4.21)$$

$$\underline{\mathbf{p}} \leq \mathbf{p} \leq \bar{\mathbf{p}} \quad (4.22)$$

$$\begin{aligned} \underline{\mathbf{f}}_\tau^M &\leq \mathbf{g}_\tau^0 + \hat{\Psi}_\tau^M (\mathbf{p} - \mathbf{l}) - \\ &\hat{\Phi}_\tau^{MZ} \mathbf{v}_\tau^Z + \hat{\Phi}_\tau^{MS} \mathbf{v}_\tau^S \leq \bar{\mathbf{f}}_\tau^M \end{aligned} \quad (4.23)$$

$$\tilde{\mathbf{F}}_\tau \mathbf{t}^S \leq \hat{\Psi}_\tau^S (\mathbf{p} - \mathbf{l}) + \left(\hat{\Phi}_\tau^{SS} - \mathbf{I} \right) \mathbf{v}_\tau^S -$$

$$\hat{\Phi}_\tau^{SZ} \mathbf{v}_\tau^Z \leq \tilde{\mathbf{F}}_\tau \mathbf{t}^S \quad (4.24)$$

$$\begin{aligned} -M(\mathbf{1} - \mathbf{t}^Z) \leq \mathbf{A}_\tau^Z \mathbf{B}_\tau^{-1} \left(\mathbf{A}_\tau^{Z'} \mathbf{v}_\tau^Z + (\mathbf{p} - \mathbf{1}) - \right. \\ \left. \mathbf{A}_\tau^{Z'} \hat{\Phi}_\tau^{MS} \mathbf{v}_\tau^S \right) \leq M(\mathbf{1} - \mathbf{t}^Z) \end{aligned} \quad (4.25)$$

$$-M(\mathbf{1} - \mathbf{t}^S) \leq \mathbf{v}_\tau^S \leq M(\mathbf{1} - \mathbf{t}^S) \quad (4.26)$$

$$-M\mathbf{t}^Z \leq \mathbf{v}_\tau^Z \leq M\mathbf{t}^Z \quad (4.27)$$

$$t^Z, t^S \in \{0, 1\} \quad (4.28)$$

Where equation (4.24) forces the flow on opened branches to zero. The formulation above allow us to model both branch switching and breaker closing with a single optimization problem.

4.2 Breaker Opening Incremental Flows

To formulate a linear shift factor based OPF that emulates the opening of breakers we would like to use flow-cancelling transactions. Unfortunately, the use of FCTs creates two problems. In the branch opening formulation we isolate the branch to be opened and introduce a FCT, v , at the ends of this branch, which has the same impact on the rest of the system as actually opening the branch. The algorithm determines v by implicitly calculating the LODF, which requires evaluating $(\mathbf{I} - \Phi^{SS})^{-1}$. For breakers this expression is undefined since the self PTDF matrix, Φ^{SS} is 1.

The second problem arises from the impact of FCTs on the rest of the system. Due to the self PTDF being 1, we cannot introduce FCTs at the ends of the breakers whose opening we want to emulate. If we try to introduce FCTs at any other nodes in the system we would inadvertently impact nodal balance constraints. Figure 4.1 illustrates this problem. By design the FCT is balanced so it does not change the system-wide energy balance constraint. However, the FCT should have the same impact on all other branches as actually opening the breaker and we must satisfy nodal balance in both networks. From

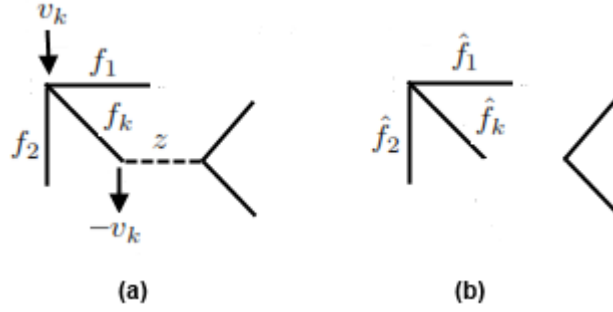


Figure 4.1: (a) shows part of a network with a breaker z and an FCT v across branch k that we assume is necessary to emulate the opening of breaker z . The resulting flows on the 3 branches are labelled. (b) shows the network with the breaker physically opened and the resulting flows on the 3 branches

figure 4.1 this implies the following conditions:

$$\begin{aligned}
 f_1 &= \hat{f}_1 \\
 f_2 &= \hat{f}_2 \\
 f_3 &= \hat{f}_3 \\
 f_1 + f_2 + f_3 + v_k &= 0 \\
 \hat{f}_1 + \hat{f}_2 + \hat{f}_3 &= 0
 \end{aligned}$$

Clearly these constraints cannot be mutually satisfied. The two problems preclude the use of FCTs for emulating the opening of breakers. To get around these issues we work directly with fictitious flows that we call breaker opening incremental flows (BOIFs). The BOIF δ_ℓ^z is a fictitious flow introduced on branch ℓ , in a topology where the breaker z is connected. It is defined as the change in flow on branch ℓ when z is disconnected (similarly to a LODF) but, as explained below, avoids the problem of the self PTDF being 1. Additionally, fictitious flows do not create any nodal injections and therefore avoid the issue with the nodal balance constraints described above.

To show that BOIFs are well defined, let us take a breaker z defined from node i to j , which we express as $z = (i, j)$. Let us take any pair of branches that are incident to

breaker z , $\ell = (m, i)$ and $k = (n, i)$ and look at the per-unit impact of opening breaker z on the flow of these branches. Clearly this is just the LODF:

$$\Delta f_\ell^z = \text{LODF}_\ell^z \quad (4.29)$$

$$\Delta f_k^z = \text{LODF}_k^z \quad (4.30)$$

As stated earlier, the LODF for a breaker is undefined. However, we claim that the ratio of (4.29) to (4.30), i.e.

$$\frac{\Delta f_\ell^z}{\Delta f_k^z} = \frac{\text{LODF}_\ell^z}{\text{LODF}_k^z} = \frac{\Phi_\ell^z}{\Phi_k^z} \quad (4.31)$$

is well defined and independent of the impedance (and therefore susceptance) of z .

Theorem 4.2.1. $\frac{\Delta f_\ell^z}{\Delta f_k^z}$ is independent of the susceptance of breaker z

Proof. We first simplify the ratio and expand it in terms of the nodal susceptance matrix

$$\begin{aligned} \frac{\Delta f_\ell^z}{\Delta f_k^z} &= \frac{\text{LODF}_\ell^z}{\text{LODF}_k^z} = \frac{\phi_\ell^z}{\phi_k^z} = \\ &= \frac{\tilde{b}_\ell(B_{m,i}^{-1} - B_{i,i}^{-1} - B_{m,j}^{-1} + B_{i,j}^{-1})}{\tilde{b}_k(B_{n,i}^{-1} - B_{i,i}^{-1} - B_{n,j}^{-1} + B_{i,j}^{-1})} \end{aligned} \quad (4.32)$$

Next, we express the nodal susceptance matrix in the following block form to explicitly confine all terms containing the susceptance, \tilde{b}_z , of the breaker to a small submatrix:

$$\mathbf{B} = \begin{bmatrix} \hat{\mathbf{B}} & \mathbf{b} \\ \mathbf{b}' & \mathbf{C} \end{bmatrix} \quad (4.33)$$

$\hat{\mathbf{B}}$ represents the nodal susceptance matrix with rows and columns i, j removed, \mathbf{b} corresponds to columns i, j in the nodal susceptance matrix and \mathbf{C} is a 2x2 sub-matrix corre-

sponding to rows and columns i, j . Given the structure of the nodal susceptance matrix,²

$$(\mathbf{B})_{ii} = \sum_{\ell \in i} \tilde{b}_\ell \quad (4.34)$$

$$(\mathbf{B})_{ij} = \mathbf{1}_{(\ell=(i,j))}(-\tilde{b}_\ell) \quad (4.35)$$

\mathbf{C} can be expressed as

$$\mathbf{C} = \begin{bmatrix} \tilde{b}_z + c & -\tilde{b}_z \\ -\tilde{b}_z & \tilde{b}_z + d \end{bmatrix} \quad (4.36)$$

where c and d are some values that do not depend on \tilde{b}_z . We now apply Woodbury's matrix inversion lemma to get an explicit value for the ratio of PTDFs. Note that all the values required in (4.32) are in the sub-matrices \mathbf{b} and \mathbf{C} . The inverse of both of these blocks are given by the equation below

$$\begin{bmatrix} \dots & -\hat{\mathbf{B}}^{-1}\mathbf{b}(\mathbf{C} - \mathbf{b}'\hat{\mathbf{B}}^{-1}\mathbf{b})^{-1} \\ \dots & (\mathbf{C} - \mathbf{b}'\hat{\mathbf{B}}^{-1}\mathbf{b})^{-1} \end{bmatrix} \quad (4.37)$$

and both require the inverse of $(\mathbf{C} - \mathbf{b}'\hat{\mathbf{B}}^{-1}\mathbf{b})$, which has a form similar to (4.36).

$$(\mathbf{C} - \mathbf{b}'\hat{\mathbf{B}}^{-1}\mathbf{b}) = \begin{bmatrix} \tilde{b}_z + g & -\tilde{b}_z - e \\ -\tilde{b}_z - e & \tilde{b}_z + h \end{bmatrix} \quad (4.38)$$

Since this is a 2x2 matrix we can express the inverse as

$$(\mathbf{C} - \mathbf{b}'\hat{\mathbf{B}}^{-1}\mathbf{b})^{-1} = \frac{1}{\det} \begin{bmatrix} \tilde{b}_z + h & \tilde{b}_z + e \\ \tilde{b}_z + e & \tilde{b}_z + g \end{bmatrix} \quad (4.39)$$

Using (4.39) we can now express the terms in (4.32). We expand only the numerator in

²The notation $\ell \in i$ means all branches ℓ that are incident to node i . The indicator function $\mathbf{1}_{(\ell=(i,j))}$ is 1 when branch ℓ connects nodes i and j .

(4.40), the denominator has the same structure. The subscripts m, n refer to the row index.

$$\begin{aligned} \Delta f_\ell^z = & \tilde{b}_\ell \left(-\frac{1}{\det} \hat{\mathbf{B}}_m^{-1} \mathbf{b} \begin{bmatrix} b_z + h \\ b_z + e \end{bmatrix} - \frac{1}{\det} (b_z + h) \right. \\ & \left. + \frac{1}{\det} \hat{\mathbf{B}}_m^{-1} \mathbf{b} \begin{bmatrix} b_z + e \\ b_z + g \end{bmatrix} + \frac{1}{\det} (b_z + e) \right) \end{aligned} \quad (4.40)$$

All terms are multiplied by $\frac{1}{\det}$, which cancel with the same term in the denominator. Further, all terms that multiply b_z in (4.40) cancel out and we are left with an expression that no longer depends on the susceptance of the breaker.

$$\frac{\Delta f_\ell^z}{\Delta f_k^z} = \frac{\tilde{b}_\ell \left(\hat{\mathbf{B}}_m^{-1} \mathbf{b} \begin{bmatrix} h + e \\ e + g \end{bmatrix} + h - e \right)}{\tilde{b}_k \left(\hat{\mathbf{B}}_n^{-1} \mathbf{b} \begin{bmatrix} h + e \\ e + g \end{bmatrix} + h - e \right)} \quad (4.41)$$

While explicitly calculating the above expression for every breaker is impractical, we do not need to do so. By replacing the infinite susceptance of the breaker with an arbitrary finite number, we can calculate an auxiliary PTDF matrix, $\hat{\mathbf{\Phi}}$ and use it to find the ratios in (4.32). \square

Taking advantage of this claim, we show in the next section that we can find fictitious incremental flows for all branches incident to z that emulate the opening of breaker z . Further, these BOIFs impact the rest of the system in the same way as physically opening z .

4.3 BOIF Formulation

Using the ratio of incremental flows derived in the previous section, we can formulate a shift factor based MIP OPF to optimize the opening of breakers. To motivate this formulation,

figure 4.2 below shows an illustrative 6-bus model that will help visualize the necessary constraints. We can think of opening a zero-impedance breaker as separating busbars from

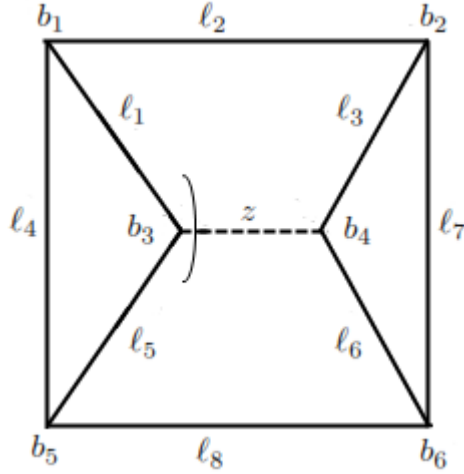


Figure 4.2: small 6-bus network with branches labeled as ℓ_1 through ℓ_8 and busses b_1 through b_6 .

a substation. With breaker z closed, busbars b_3 and b_4 can be collapsed into a single busbar. If we open breaker z , we introduce a “substation cutset”, shown by the arc in figure 4.2 and separate busbar b_3 from the rest of the substation (in this case we also separate busbar b_4). From the previous section we know that to find the impact of opening z on the rest of the system, we must consider the relative changes in flow for any pair of branches. Applying this result, we introduce a BOIF variable, $\delta^z = \Delta f_{\ell_1}^z$ representing the change in flow on ℓ_1 when breaker z is opened. We call ℓ_1 the reference branch and calculate the changes in flow on branches incident to the from node of breaker z . From (4.31) we have:

$$\delta_k^z = \delta^z \frac{\hat{\Phi}_k^z}{\hat{\Phi}_{\ell_1}^z} = \delta^z \gamma_k^z \quad k = \ell_5 \quad (4.42)$$

Equation (4.42) establishes a relationship between changes in flows that would result from the opening of breaker z . In addition, we need to determine the magnitude of δ^z . In the post-open topology, the total flow through branches ℓ_1 and ℓ_5 will be zero. In the pre-open topology our BOIF should emulate this condition. Equation (4.43) expresses this

constrain.³

$$\begin{aligned}
 -Mt_z &\leq \sum_{\ell \in (\ell_1, \ell_5)} \left(\Psi^\ell(\mathbf{p} - \mathbf{1}) + \delta_\ell^z \right) + \\
 &\quad + l_3 - p_3 \leq Mt_z
 \end{aligned} \tag{4.43}$$

This equation is a nodal balance constraint for busbar b_3 in the pre-open network, except that we replace the flow through breaker z with the fictitious breaker opening incremental flows (BOIFs) that emulate its opening. We take a moment here to make two key observations. First, we can combine (4.42) and (4.43). Second, equation (4.43) balances only one of the two busbars we separated. This is a sufficient condition. If the flow through branches ℓ_1 and ℓ_5 is 0, the flow through branches ℓ_3 and ℓ_6 will naturally satisfy the same condition.

The example above illustrates the constraints required to model the opening of a single breaker. In the rest of this section we expand these constraints to allow for multiple breakers.

If we introduce a second breaker, z_2 , not connected to z_1 , equation (4.43) becomes:

$$\begin{aligned}
 -Mt_z &\leq \sum_{\ell \in (\ell_1, \ell_5)} \left(\Psi^\ell(\mathbf{p} - \mathbf{1}) + \delta^1 \gamma_\ell^1 + \delta^2 \gamma_\ell^2 \right) + \\
 &\quad + l_3 - p_3 \leq Mt_z
 \end{aligned} \tag{4.44}$$

Note that we only consider the reference branch for z_2 when calculating the impact on the nodal balance constraint for z_1 . To see that this is indeed the case, consider an arbitrary set of injections that cause a δ_k change in the flow on some branch, k . We can use shift factors to calculate their impact on other branch, ℓ but we can also use PTDFs and δ_k directly to get the same result.

Extending (4.44) to multiple breakers, combining (4.42) and (4.43) and changing to

³without loss of generality, (4.43) assumes that all branches incident to the from node, 3, of breaker z are defined as originating at node 3

matrix notation we have

$$\begin{aligned}
 -Mt_z &\leq \mathbf{1}'_{\ell \in i_z, \ell \notin Z} \left(\Psi(\mathbf{p} - \mathbf{1}) + \Gamma \delta \right) + \\
 &\quad + (l_{i_z} - p_{i_z}) \leq Mt_z \quad \forall z
 \end{aligned} \tag{4.45}$$

Where $\mathbf{1}_{\ell \in i_z, \ell \notin Z} = 1$ when branch ℓ originates or terminates at the from node, i_z , of breaker z and is not itself a breaker.

Next we consider the case of multiple breakers. Figure 4.3 shows a stylized ring bus configuration but the same principle applies to breaker-and-a-half or double bus double breaker configurations. As mentioned earlier, when considering switching breakers we are

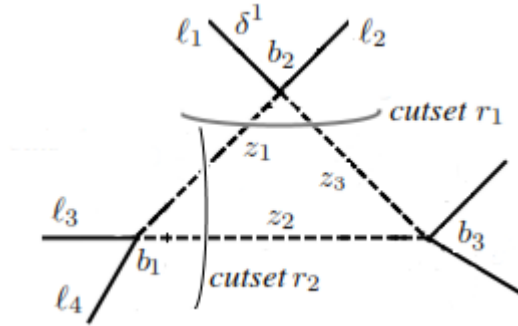


Figure 4.3: Stylized ring bus configuration.

really considering the set of busbars at the ends of the breakers. In figure 4.3 opening any single breaker has no impact on the rest of the system. It is more intuitive to think about substation configurations, which in turn lead to a set of candidate breakers. In the figure above, if we chose to separate busbar b_2 , this requires jointly opening breakers z_1 and z_3 and these decisions should be coupled. To do this, we introduce a new index r that refers to a substation cutset that will separate a busbar from a substation. We refer to the separation of one or multiple busbars as a substation configuration. Let us consider two cutsets in figure 4.3. The first, r_1 , consists of branches ℓ_1 and ℓ_2 , and the second, r_2 consists of ℓ_3 and ℓ_4 . We additionally impose a rule that only one of these cutsets may be

implemented. Our constraint set for this case would be

$$\begin{aligned}
-Mt_r &\leq \mathbf{1}'_{\ell \in r, \ell \notin Z} (\Psi(\mathbf{p} - \mathbf{1}) + \Gamma\boldsymbol{\delta}) \\
&\quad + (l_r - p_r) \leq Mt_r
\end{aligned} \tag{4.46}$$

$$-M(1 - t_r) \leq \boldsymbol{\delta} \leq M(1 - t_r) \quad \forall r, \boldsymbol{\delta} \in r \tag{4.47}$$

$$t_1 + t_2 \leq 1 \tag{4.48}$$

Equation (4.46) is similar to (4.45) except that our binary variables are now cutset dependent and can couple the opening of multiple breakers. l_r and p_r refer to load and generation at the substation where the branches in r are connected⁴. Equation (4.47) is a standard big-M constraint that allows the BOIFs to be freely set by (4.46) when a particular busbar is disconnected from the substation. The notation $z \in r$ refers to the breakers belonging to cutset r that would be opened. Finally, (4.48) enforces the rule that only one busbar can be separated from the substation. More generally, for each substation there may be a combination of technical or business rules that limit the set of possible configurations, especially if two configurations consist of cutsets with an overlapping set of breakers. All of these rules can be represented by simple relationships between the binary variables and we call the set of these rules (constraints) \mathcal{C} . We are now ready to present the full security-constrained BOIF MIP formulation

$$\mathcal{C} = \min_{\mathbf{p}, \boldsymbol{\delta}, \mathbf{t}} \mathbf{c}'\mathbf{p} \tag{4.49}$$

$$\text{s.t. } \mathbf{1}'(\mathbf{p} - \mathbf{1}) = 0 \tag{4.50}$$

$$\underline{\mathbf{p}} \leq \mathbf{p} \leq \bar{\mathbf{p}} \tag{4.51}$$

$$\underline{\mathbf{f}}_{\tau}^{\mathcal{M}} \leq \mathbf{g}_{\tau}^0 + \Psi_{\tau}^{\mathcal{M}}(\mathbf{p} - \mathbf{1}) + \Gamma_{\tau}^{\mathcal{M}}\boldsymbol{\delta}_{\tau} \leq \bar{\mathbf{f}}_{\tau}^{\mathcal{M}} \quad \forall \tau \tag{4.52}$$

$$-Mt_r \leq \mathbf{1}'_{\ell \in r, \ell \notin Z} (\Psi_{\tau}(\mathbf{p} - \mathbf{1}) + \Gamma_{\tau}\boldsymbol{\delta}_{\tau})$$

⁴For the substation reconfigurations we assume that the location of the generation and load within a substation is fixed or that it is implicitly adjusted for the configuration being considered

$$+(l_r - p_r) \leq Mt_r \quad \forall r, \tau \quad (4.53)$$

$$-M(1 - t_r) \leq \boldsymbol{\delta}_\tau \leq M(1 - t_r) \quad \forall r, \tau, \boldsymbol{\delta}_\tau \in r \quad (4.54)$$

$$\mathbf{t} \in C \quad (4.55)$$

$$\mathbf{t} \in \{0, 1\} \quad (4.56)$$

We stated earlier that this formulation can handle any substation configuration and that loops formed by breakers do not create a problem. Indeed, the BOIF formulation does not rely on shift factors for breakers. Therefore when calculating shift factors, $\boldsymbol{\Psi}_\tau$, we can first consolidate substations into equivalent buses and then calculate standard shift factors. From the perspective of the rest of the system, including breakers that form a loop makes no impact.

4.3.1 Joint BOIF and Branch Switching Formulation

For completeness, we again present the joint formulation for breaker and branch switching.

$$C = \min_{\mathbf{p}, \boldsymbol{\delta}, \mathbf{t}^{\mathcal{F}}, \mathbf{t}^{\mathcal{S}}, v} \mathbf{c}'\mathbf{p} \quad (4.57)$$

$$\text{s.t. } \mathbf{1}'(\mathbf{p} - \mathbf{l}) = 0 \quad (4.58)$$

$$\underline{\mathbf{p}} \leq \mathbf{p} \leq \bar{\mathbf{p}} \quad (4.59)$$

$$\begin{aligned} \mathbf{f}_\tau^{\mathcal{M}} &\leq \mathbf{g}_\tau^0 + \boldsymbol{\Psi}_\tau^{\mathcal{M}}(\mathbf{p} - \mathbf{l}) \\ &+ \boldsymbol{\Gamma}_\tau^{\mathcal{M}}\boldsymbol{\delta}_\tau + \boldsymbol{\Phi}_\tau^{\mathcal{MS}}\mathbf{v}_\tau \leq \bar{\mathbf{f}}_\tau^{\mathcal{M}} \quad \forall \tau \end{aligned} \quad (4.60)$$

$$\begin{aligned} -Mt_r &\leq \mathbf{1}'_{\ell \in i_r, \ell \notin \mathcal{Z}} \left(\boldsymbol{\Psi}_\tau(\mathbf{p} - \mathbf{l}) + \boldsymbol{\Gamma}_\tau\boldsymbol{\delta}_\tau \right. \\ &\left. + \boldsymbol{\Phi}_\tau^{\mathcal{MS}}\mathbf{v}_\tau \right) + (l_r - p_r) \leq Mt_r \quad \forall r, \tau \end{aligned} \quad (4.61)$$

$$\begin{aligned} \tilde{\mathbf{F}}_\tau \mathbf{t}^{\mathcal{S}} &\leq \boldsymbol{\Psi}_\tau^{\mathcal{S}}(\mathbf{p} - \mathbf{l}) + (\boldsymbol{\Phi}_\tau^{\mathcal{SS}} - \mathbf{I})\mathbf{v}_\tau \\ &+ \boldsymbol{\Gamma}_\tau^{\mathcal{S}}\boldsymbol{\delta}_\tau \leq \tilde{\mathbf{F}}_\tau \mathbf{t}^{\mathcal{S}} \quad \forall \tau \end{aligned} \quad (4.62)$$

$$-M(\mathbf{1} - \mathbf{t}^{\mathcal{S}}) \leq \mathbf{v}_\tau^{\mathcal{S}} \leq M(\mathbf{1} - \mathbf{t}^{\mathcal{S}}) \quad \forall \tau \quad (4.63)$$

$$-M(\mathbf{1} - \mathbf{t}^{\mathcal{R}}) \leq \boldsymbol{\delta}_\tau \leq M(\mathbf{1} - \mathbf{t}^{\mathcal{R}}) \quad \forall r, \tau, \boldsymbol{\delta}_\tau \in r \quad (4.64)$$

$$\mathbf{t}^{\mathcal{R}} \in \mathcal{C} \quad (4.65)$$

$$\mathbf{t}^{\mathcal{R}}, \mathbf{t}^{\mathcal{S}} \in \{0, 1\} \quad (4.66)$$

In equation (4.61) we assume that branches incident to breakers are in the monitored set but this need not be the case. Formulation (4.57)-(4.66) starts from the original topology and allows for re-configuration of substations and branch switching within a single MIP formulation.

4.4 Breaker Modeling

In this section we discuss practical applications for the BCT and BOIF formulations, evaluate their performance on a real system and looks at the joint benefit of breaker and branch opening. For the test system, we use a subarea of the PJM system and compare the production cost savings, solution times and applicability of each formulation. We show that both substation reconfiguration formulations can achieve comparable savings to the FCT formulation for branch opening/closing. This is encouraging because the set of breakers that can be opened or closed is small compared to the equivalent set of branches. In the test system we consider all breakers that split a bus (generally consistent with PJM practices) to be switchable and using this set we can solve both the BOIF and BCT formulations to optimality. Solving the FCT formulation would require the use of heuristics to identify a set of candidate branches before a MIP could be solved. While our previous work [17] shows that such heuristics can achieve very good solutions, being able to solve a MIP is always preferable. For larger systems and with inclusion of contingency constraints some heuristics may be necessary to limit the number of candidate breakers, however, the initial set is relatively small and we expect that such a limited set could be included directly in the BOIF or BCT MIPs.

Substation reconfigurations are viewed as a less disruptive change compared to branch opening, and for those, the time required analyze, coordinate and implement the topology

change could be significantly less than the time for branch openings. Moreover, including breaker opening/closing in combination with other topology control actions provides system operators additional mechanisms for managing congestion, responding to contingency events or accommodating transmission maintenance requests. From a performance perspective we demonstrate that both the BCT and BOIF formulations can be solved quickly. While we do not consider contingency constraints in the results presented here, the MIP solve times are comparable to equivalent FCT models without contingencies. Since both of the breaker formulations rely on the same shift factor representation of flows as the FCT formulation for branch switching, we expect them to scale similarly with the addition of contingencies [31].

In order to implement the BCT formulation we need to store the nodal susceptance matrix for every contingent topology. As shown in the companion paper, once the base topology nodal susceptance matrix is calculated we can efficiently update it for contingent topologies. In order to minimize data storage we can use the resulting nodal susceptance matrices to calculate shift factor matrices in an additional pre-processing step or, since contingent topologies are known up front, all nodal susceptance and shift factor matrices can be calculated externally and read into the model directly. Regardless of the approach, the additional data storage requirements compared to a standard shift factor OPF model is T , $N \times N$ nodal susceptance matrices where T is the number of topologies and N the number of busses.

While the BOIF model is more flexible by not imposing non-islanding conditions on the selection of candidate breakers, there is additional overhead in the amount of data that needs to be pre-calculated. For each breaker and contingent topology we will have a vector of ratios. These calculations can be performed in a preprocessing step or, all contingencies can be represented through flow cancelling transactions. This allows us to model the impact of a contingency on other branches using flows (product of PTDF and FCT). Such incremental flows are additive and can be combined with BOIFs, allowing us to maintain PTDF ratios for only the base topology.

4.4.1 BOIF and BCT Applications

Both substation reconfiguration formulations discussed in this chapter provide additional tools for system operators to better manage the operation of power markets. The BCT formulation could be used to restore feasibility following a contingency event or for short-term transmission maintenance planning. System operators often get dozens of maintenance requests from transmission owners, which are verified one at a time to ensure the request does not cause reliability violations. The state of the network would typically have a set of breakers opened. In most cases this set would be small and using the BCT formulation would allow the system operator to quickly find a small number of breakers whose closing could resolve transmission violations caused by the maintenance request. The BCT formulation requires less overhead compared to the BOIF formulation with minimal preprocessing compared to a standard OPF formulation. In general, when a set of breakers is already open or when opening additional branches or breakers is not desired, solving the BCT formulation to reduce the cost of congestion or to restore feasibility following a contingency could be done quickly and efficiently.

Despite these advantages, the BCT formulation requires candidate breakers to be open, limiting the set of topology configurations that can be considered since opening certain combinations of breakers can create islands. This is especially a concern in the presence of contingencies where the opening of all candidate breakers would have to maintain a connected network under every contingent topology. If the system operator's goal is to identify promising (from cost saving or overload relief perspectives, for example) an alternative formulation, such as the BOIF formulation, becomes necessary. Since the BOIF formulation starts with a topology where candidate breakers are closed we can consider any of them as switchable because there are no initial connectivity restrictions on the set of switchable breakers and by definition, the formulation cannot switch any breakers that would result in islanding. The BOIF formulation may be able to identify more efficient reconfigurations than the BCT formulation, especially under complex congestion conditions. With

the BOIF formulation we can also consider multiple configurations of a single substation simultaneously, allowing the MIP solver to decide which is more beneficial. This flexibility comes at the expense of additional overhead and data storage described above.

4.4.2 Substation Test System

The test system used in all simulations represents 168 hours in a historical 2013 week of a subarea of PJM. Each hour was modeled independently with the assumption that each breaker can be opened/re-closed in each hour. The system can be further characterized as follows:

- 2,264 branches (298 monitored)
- 2,034 nodes
- 63 generators
- Hourly loads, generator commitment schedules and costs taken from the EMS
- Contingency constraints are not included

Out of all zero-impedance breakers, we identified 57 whose opening would split a bus. In the test system used, all 57 breakers could not be opened at the same time without splitting the system. Therefore, a subset of 41 switchable breakers that do not island the system when opened simultaneously was selected. Since all candidate breakers are open under the BCT formulation, the remaining substations can be collapsed into their representative busses and this significantly reduces the number of breakers modeled explicitly. After performing this consolidation, the model size is reduced to only 406 branches and 310 busses. In the BOIF formulation we could use all 57 candidate breakers. However, for comparability of results with the BCT formulation we maintain the same 41 candidates for both formulations.

In addition to modeling the BOIF and BCT formulations we also model the FCT formulation and provide results for the joint BOIF and FCT formulation. Since there are

over 400 branches in the reduced test system we cannot consider all of them as switchable. Prior to running the FCT model we evaluate the price difference policy to determine a set of candidate branches (the details of this policy can be found in [20]). For each hour, the price difference policy performs the following steps:

1. Rank all branches using the metric: $sign(f_\ell)(LMP_{\ell_{To}} - LMP_{\ell_{From}})$
2. Open top ranked branch and solve OPF
3. Compare post-open to pre-open production costs. If there is an improvement, keep branch from step 2 open in all future iterations and go to step 1. Otherwise end and go to next hour.

This algorithm generated five candidate branches for the week simulated, which were included in the switchable set for each hourly MIP model. Note that there may be other branches whose opening would produce savings but our goal here is to quickly generate a reasonable switchable set.

In evaluating the performance of the BCT, BOIF and joint BOIF+FCT formulation, the next section presents results comparing the number of topology control actions across the models as well as solution times and cost of congestion savings. The cost of congestion savings are calculated using the following metric, which looks at savings achieved relative to the maximum possible savings and makes the comparison across hours more consistent:

$$\%savings = \frac{C^{full\ topology} - C^{optimized\ topology}}{C^{full\ topology} - C^{no\ constraints\ topology}} \quad (4.67)$$

All of the modeling was implemented in AIMMS 3.12 using CPLEX 12.5 with default settings. Simulations were run on a 64-bit workstation with two 2.93 GHz Intel Xeon processors (8 cores total) and 24 GB of RAM. Due to the small system size, the MIP models were solved to optimality and a value of 5000 was used for M in the formulations.

4.4.3 Simulation Results

Figure 4.4 shows a summary of breakers opened/kept open by the BOIF/BCT formulations respectively. Because the size of the system is relatively small and we are not including

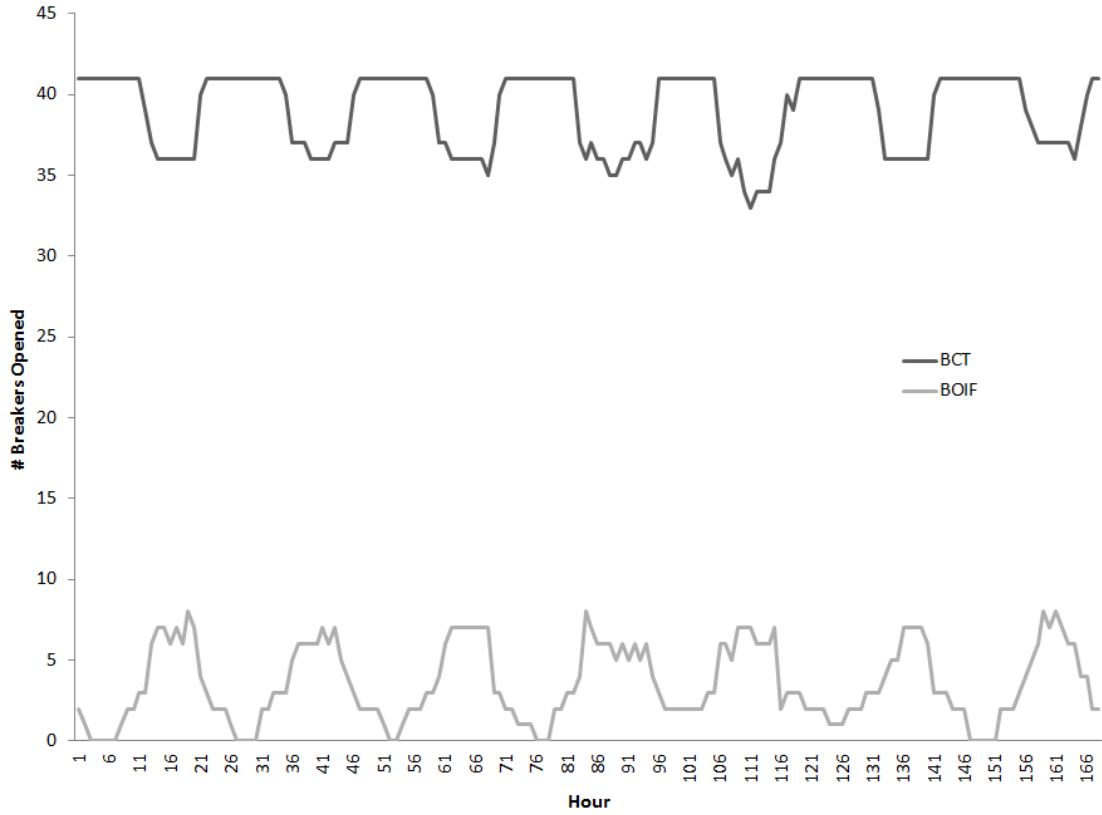


Figure 4.4: Breakers kept open in the breaker closing transaction (BCT) formulation and breakers opened in the breaker opening incremental flow (BOIF) formulation.

contingency constraints, we are able to solve both models to the global optimal (a MIP gap of 0%). From Figure 4.4 we see that the number of breakers left open in the final hourly topologies are different between the BCT and BOIF formulations, indicating that there are multiple optimal topologies in the test system considered. To better compare the number of breakers operated in the two models, figure 4.5 shows the number of breakers closed in the BCT model. In most hours the BCT model operates fewer breakers, which is further summarized in Table 4.1. These results are, of course, conditional on the level

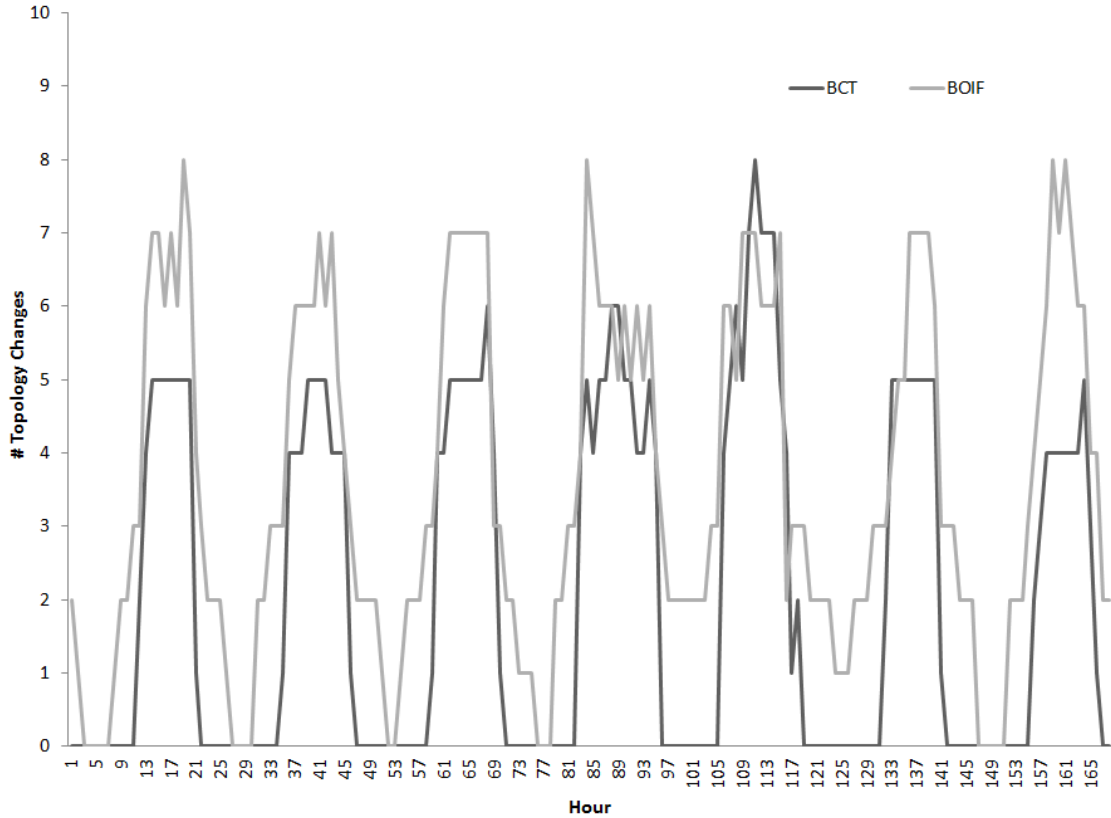


Figure 4.5: Number of breakers operated in the BCT and BOIF models

of congestion in the network. Given the fairly light system conditions due to not enforcing contingency constraints, in many off-peak hours having all candidate breakers open is an optimal solution. If system conditions were more strained, having all candidate breakers open would cause violations in many more hours requiring additional breaker closings under the BCT model. However, these results demonstrate that under light congestion and when a set of breakers is already open, the BCT model may be preferable to the BOIF one in terms of the number of topology changes.

Figure 4.6 and table 4.1 compare solution times for the two formulations. While both formulations solve quickly, the BCT model solves faster on average, especially in off-peak hours. From Figures 4.5 and 4.6 we see, as expected, a general correlation between the number of topology changes and the solve time. This further enforces the claim that under

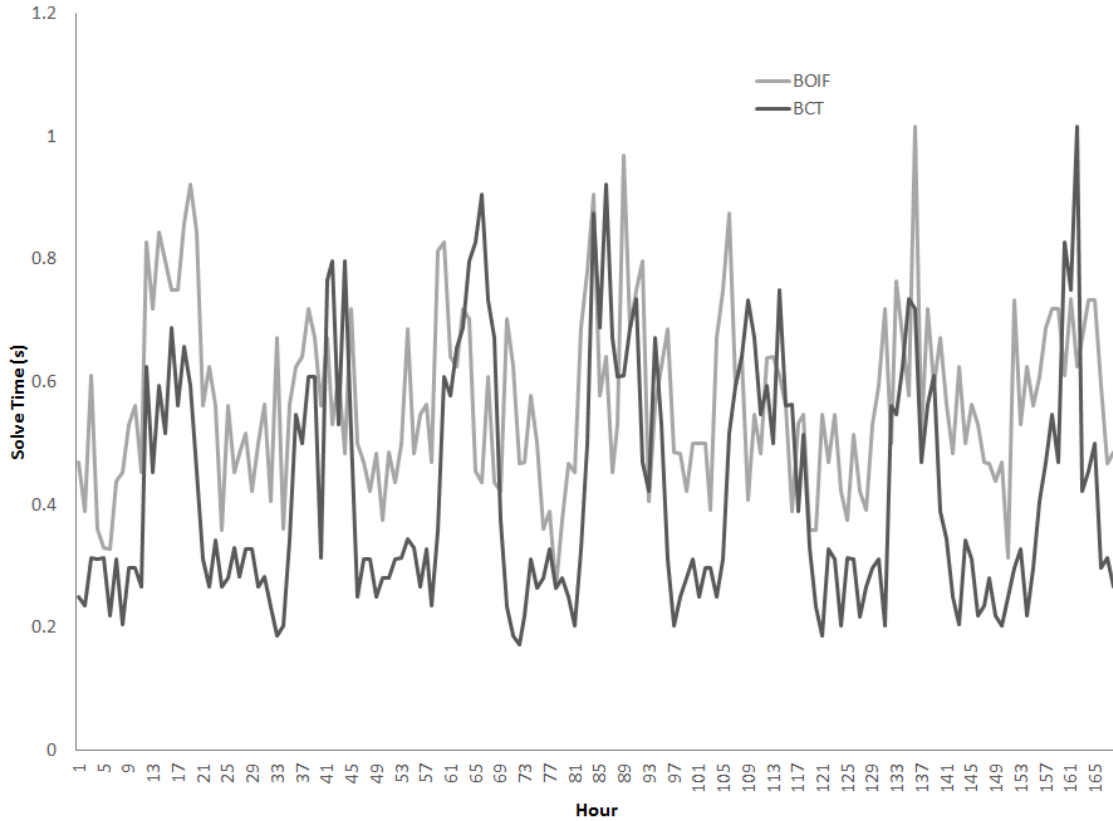


Figure 4.6: Solve times, reported in seconds, for the BCT and BOIF formulations

certain system conditions the BCT model may be the appropriate formulation to use.

Table 4.1: BOIF and BCT Solve Times (seconds)

	BCT	BOIF
Min	0.172	0.265
Max	1.02	1.02
Avg	0.42	0.57

Next, we consider the joint FCT and BOIF formulation and compare the performance of this joint model to the individual FCT and BOIF formulations⁵. Figure 4.7 shows the number of branch and breaker openings for the three models. We observe that the joint and FCT formulations perform the same number of topology changes. One reason for this

⁵Since the BCT and BOIF formulations lead to the same production cost savings, we only consider the joint BOIF+FCT model here.

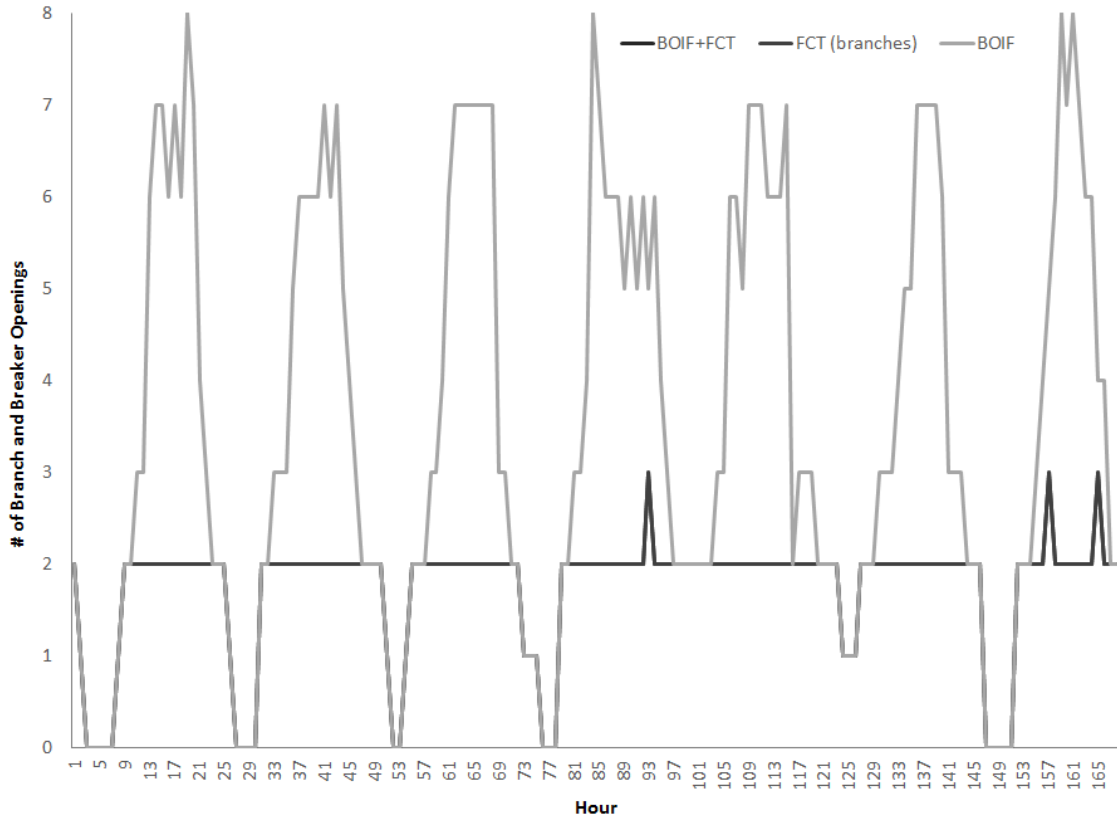


Figure 4.7: Branch and breaker openings under the BOIF, FCT and joint formulations

is the limited congestion in the system combined with the selection process for switchable branches and breakers. For branches we evaluated all branches using the price difference policy, whereas for breakers we simply fixed the switchable set to a subset of breakers that split a bus. Despite this result, however, Table 4.2 shows that the joint formulation opens fewer breakers and branches than the FCT or BOIF models individually. This is clearly beneficial to system operators since fewer changes are required to the state of the network. Additionally, this shows that in many hours a breaker opening can serve as a substitute for a branch opening, which can give system operators multiple options for handling certain congestion or contingency events.

Figure 4.8 shows cost of congestion savings for the three models. In addition to reducing the number of topology changes compared to the FCT or BOIF formulation, the joint

Table 4.2: Topology Control Actions in the BCT, BOIF, FCT and Joint BOIF+FCT formulations

	BCT (closings)		BOIF	FCT	BOIF+FCT (breakers)	BOIF+FCT (branches)
Min	0	0	0	0	0	0
Max	8	8	3	2	2	2
Avg	2.08	3.56	1.7	.45	1.3	1.3

BOIF+FCT formulation achieves greater cost of congestion savings in peak hours. Since

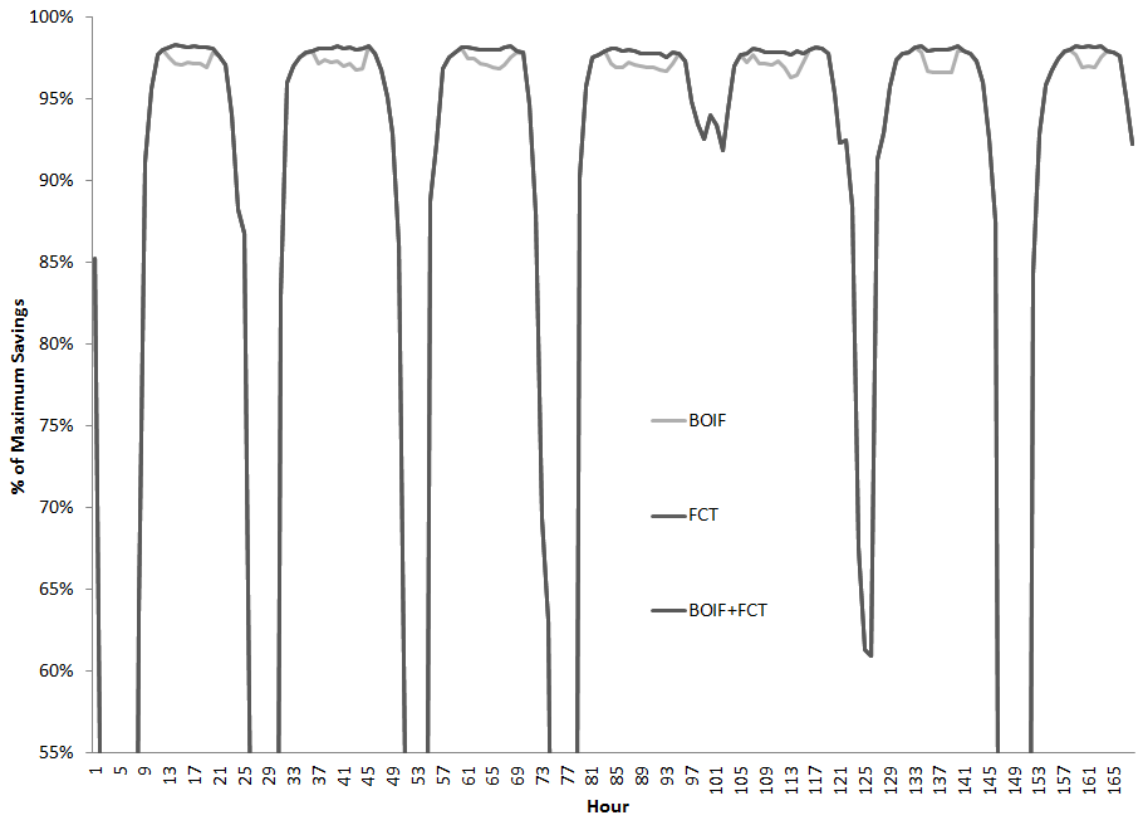


Figure 4.8: Cost of Congestion Savings (%) for the BOIF, FCT and joint formulations

we are not modeling contingency constraints all of the formulations are able to almost entirely relieve network congestion, especially during off-peak hours where both achieve the same savings. We note again that for comparability of results we unnecessarily restricted the set of switchable breakers in the BOIF model. Given the percent savings achieved in most hours it is unlikely that the additional breakers would provide much benefit but in

general we expect the BOIF model to generate more savings than the BCT model. We mentioned before that only breakers that split a bus were considered as switchable. This is generally consistent with the type of breakers operated by PJM, however, being able to identify promising breakers using similar policies that exist for branch selection would be very useful. This topic has not been widely studied and is a subject of future research in this area.

Chapter 5

Concluding Remarks

This work develops a new MILP-based TC formulation based on shift factors that is consistent with the SCED and SCUC formulations currently used in practice. In contrast with the widely used $B\theta$ TC formulation, the shift factor TC formulation is compact and scales with the number of decision variables (switchable branches and breakers) and transmission constraints (monitored lines and contingencies). While the shift factor formulation is significantly denser than the $B\theta$ formulation, it solves significantly faster, especially in large systems and for TC problems with a reduced number of switchable lines where the majority of the relevant operational constraints are contingency constraints (as is the case in most practical systems).

We extended the lossless DC formulation to account for losses by deriving loss-adjusted shift factors and showing that both losses and flows can be updated linearly with changes in topology. Through simulation on the IEEE 118-bus system, we analyze the impact of losses on the DC formulation and find that both DC formulations lead to similar savings when solving the AC SCOPF. While the loss-adjusted formulation opens fewer lines both can be used reliably to assess the benefits of topology control.

In the second extension to the branch switching formulation we evaluate the impact of AC-modeling on the performance of topology control algorithms. For TC to be used in ISO control rooms, it is important that our algorithms maintain AC feasibility; restoring AC feasibility once a number of topology control actions are taken can be overly time consuming in an operations setting. Therefore, we extend the original DC linearization of the OPF to include linearized constraints for reactive power and voltage and update this

linearization, including losses, at each iteration of the algorithm. The AC-based formulation is computationally more expensive than its DC counterpart and as a result tends to evaluate fewer candidate lines within the imposed five minute time constraint. Nevertheless, the results show that the relative savings captured by the AC-based TCA are substantial. In addition, the AC-based TCA opens fewer lines, which is more attractive to system operators and transmission owners from an implementation perspective. The evidence reported in [31] on the tractability of DC-based TCA in reducing congestion costs on a system the size of PJM is replicated here for the AC-based TCA, which additionally ensures the AC feasibility required for operational TC actions.

In the third extension to our TC algorithms we extend the DC formulation to model substation reconfiguration through opening and closing zero-impedance breakers. We derive a shift factor framework for modeling breakers that connect busbars within a substation and presents two MIP formulations to optimize substation configuration in the SCOPF problem. Through simulations on a subarea of the PJM system we demonstrate that both formulations can be solved efficiently and have practical applications in operations. Additionally, we show that joint modeling of breaker and branch switching can provide incremental benefits in terms of congestion cost savings and number of switches operated, compared to either branch or breaker switching alone.

Future work will focus on the development of heuristics for identifying promising breakers for switching and incorporation of substation reconfiguration into the existing AC-modeling framework. The shift-factor formulation developed here is also promising for application to transmission maintenance scheduling and transmission expansion planning, as well as chronological production cost and reliability simulation with stochastic topology (e.g., due to transmission outages) and resources [32]. In conclusion, this work provides strong evidence to support the ability of TCA to be usefully employed in both markets and operations.

Bibliography

- [1] Switching solutions. PJM Interconnection. Accessed Sep 26, 2012. [Online]. Available: <http://www.pjm.com/markets-and-operations/etools/oasis/system-information/switching-solutions.aspx>
- [2] A. Mazi, B. Wollenberg, and M. Hesse, "Corrective control of power system flows by line and bus-bar switching," *IEEE Transactions on Power Systems.*, vol. 1, no. 3, pp. 258–264, Aug. 1986.
- [3] A. G. Bakirtzis and A. P. S. Meliopoulos, "Incorporation of switching operations in power system corrective control computations," *IEEE Transactions on Power Systems.*, vol. 2, no. 3, pp. 669–675, Aug. 1987.
- [4] W. Shao and V. Vittal, "Corrective switching algorithm for relieving overloads and voltage violations," *IEEE Transactions on Power Systems.*, vol. 20, no. 4, pp. 1877–1885, Nov. 2005.
- [5] G. Schnyder and H. Glavitsch, "Security enhancement using an optimal switching power flow," *IEEE Transactions on Power Systems.*, vol. 5, no. 2, pp. 674–681, May 1990.
- [6] H. Glavitsch, "Power system security enhanced by post-contingency switching and rescheduling," in *IEEE PowerTech Conference*, Sept. 1993, pp. 16–21.
- [7] R. Bacher and H. Glavitsch, "Loss reduction by network switching," *IEEE Transactions on Power Systems.*, vol. 3, no. 2, pp. 447–454, May 1988.
- [8] S. Fliscounakis, F. Zaoui, G. Simeant, and R. Gonzalez, "Topology influence on loss reduction as a mixed integer linear programming problem," in *IEEE PowerTech Conference*, July 2007, pp. 1987–1990.
- [9] R. O'Neill, R. Baldick, U. Helman, M. Rothkopf, and W. Stewart, "Dispatchable transmission in RTO markets," *IEEE Transactions on Power Systems.*, vol. 20, no. 1, pp. 171–179, Feb. 2005.
- [10] E. B. Fisher, R. P. O'Neill, and M. C. Ferris, "Optimal transmission switching," *IEEE Transactions on Power Systems.*, vol. 23, no. 3, pp. 1346–1355, Aug. 2008.
- [11] K. W. Hedman, R. P. O'Neill, E. B. Fisher, and S. S. Oren, "Optimal transmission switching with contingency analysis," *IEEE Transactions on Power Systems.*, vol. 23, no. 3, pp. 1577–1586, Aug. 2009.

- [12] K. W. Hedman, M. C. Ferris, R. P. O'Neill, E. B. Fisher, and S. S. Oren, "Co-optimization of generation unit commitment and transmission switching with n-1 reliability," *IEEE Transactions on Power Systems.*, vol. 25, no. 2, pp. 1052–1063, May 2010.
- [13] B. Wollenberg and A. Wood, *Power Generation, Operation and Control*, 2nd ed. New York, NY: John Wiley, 1996.
- [14] T. Güler and G. Gross, "Detection of island formation and identification of causal factors under multiple line outages," *IEEE Transactions on Power Systems.*, vol. 22, no. 2, pp. 505–513, May 2007.
- [15] I. Vágó, *Graph Theory: Application to the Calculation of Electrical Networks*, ser. Studies in electrical and electronic engineering. Elsevier, 1985, pp. 31–32, 46–48.
- [16] F. Schweppe, M. Caramanis, R. Tabors, and R. Bohn, *Spot Pricing of Electricity*, ser. Power Electronics and Power Systems. Springer US, 1988.
- [17] P. A. Ruiz, J. M. Foster, A. Rudkevich, and M. C. Caramanis, "Tractable transmission topology control using sensitivity analysis," *IEEE Transactions on Power Systems.*, vol. 27, no. 3, pp. 1550–1559, Aug. 2012.
- [18] K. W. Hedman, R. P. O'Neill, E. B. Fisher, and S. S. Oren, "Optimal transmission switching - sensitivity analysis and extensions," *IEEE Transactions on Power Systems.*, vol. 23, no. 3, pp. 1469–1479, Aug. 2008.
- [19] J. Ostrowski, J. Wang, and C. Liu, "Exploiting symmetry in transmission lines for transmission switching," *IEEE Transactions on Power Systems.*, vol. 27, no. 3, pp. 1708–1709, Aug. 2012.
- [20] P. A. Ruiz, J. M. Foster, A. Rudkevich, and M. C. Caramanis, "On fast transmission topology control heuristics," in *IEEE Power & Engineering Society General Meeting*, Detroit, MI, July 2011.
- [21] J. M. Foster, P. A. Ruiz, A. Rudkevich, and M. C. Caramanis, "Economic and corrective applications of tractable transmission topology control," in *Proc. 49th Allerton Conference on Communications, Control and Computing*, Monticello, IL, Sept. 2011, pp. 1302–1309.
- [22] J. D. Fuller, R. Ramasra, and A. Cha, "Fast heuristics for transmission-line switching," *IEEE Transactions on Power Systems.*, vol. 27, no. 3, pp. 1377–1386, Aug. 2012.
- [23] T. Güler, G. Gross, and M. Liu, "Generalized line outage distribution factors," *IEEE Transactions on Power Systems.*, vol. 22, no. 2, pp. 879–881, May 2007.
- [24] A. Pizano-Martínez, C. R. Fuerte-Esquivel, and D. Ruiz-Vega, "A new practical approach to transient stability-constrained optimal power flow," *IEEE Transactions on Power Systems.*, vol. 26, no. 3, pp. 1686–1696, Aug. 2011.

- [25] P. A. Ruiz, A. M. Rudkevich, M. C. Caramanis, E. A. Goldis, E. Ntakou, and C. R. Philbrick, “Reduced MIP formulation for transmission topology control,” in *Proc. 50th Allerton Conference on Communications, Control and Computing*, Monticello, IL, Oct. 2012, pp. 1073–1079.
- [26] Proposed Manual 28 changes for marginal loss calculation using monitored facilities. PJM Interconnection. Accessed June 8, 2013. [Online]. Available: <http://www.pjm.com/media/committees-groups/committees/mrc/20100224/20100224-item-07-draft-manual-28-changes-for-marginal-loss.ashx>
- [27] E. Litvinov, T. Zheng, G. Rosenwald, and P. Shamsollahi, “Marginal loss modeling in LMP calculation,” *IEEE Transactions on Power Systems.*, vol. 19, no. 2, pp. 880–888, May 2004.
- [28] F. Zaoui, S. Fliscounakis, and R. Gonzalez, “Coupling OPF and topology optimization,” in *15th IEEE Power System Communications Committee*, Liege, Belgium, aug 2005.
- [29] W. Shao and V. Vittal, “BIP-Based OPF for line and bus-bar switching to relieve overloads and voltage violations,” in *Power Systems Conference and Exposition*, Atlanta, GA, Oct 2006.
- [30] J. N. Wrubel, P. S. Rapcienski, K. L. Lee, B. S. Gisin, and G. W. Woodzell, “Practical experience with corrective switching algorithm for on-line applications,” *IEEE Transactions on Power Systems.*, vol. 11, no. 1, pp. 415–421, Aug. 1996.
- [31] E. Goldis, X. Li, M. C. Caramanis, B. Keshavamurthy, M. Patel, A. Rudkevich, and P. A. Ruiz, “Applicability of topology control algorithms (TCA) to a real-size power system,” in *2013 51st Annual Allerton Conference on Communication, Control, and Computing*, Monticello, IL, Oct. 2013, pp. 1349–1352.
- [32] A. M. Rudkevich, “A nodal capacity market for co-optimization of generation and transmission expansion,” in *Proc. 50th Allerton Conference on Communications, Control and Computing*, Monticello, IL, Oct. 2012, pp. 1080–1088.

Curriculum Vitae

- Contact* Evgeniy Goldis
Division of Systems Engineering, Boston University, 15 Saint Marys Street
Brookline, MA 02446, USA
- Education* **Harvey Mudd College**, B.S., (2004) Computer Science
Boston University, M.A. (2007) Economics
Boston University PhD candidate, September 2011 – present. Thesis advisor: Michael Caramanis.
- Publications*
1. E. A. Goldis, X. Li, M. C. Caramanis, A. M. Rudkevich, P. A. Ruiz, "AC-Based Topology Control Algorithms (TCA) A PJM Historical Data Case Study." in Proceedings of the 48th Hawaii International Conference on System Sciences, January 2015
 2. Goldis, E.A. ; Caramanis, M.C. ; Philbrick, C.R. ; Rudkevich, A.M. ; Ruiz, P.A., *Security-Constrained MIP Formulation of Topology Control Using Loss-Adjusted Shift Factors*. 2014 47th Hawaii International Conference on System Sciences (HICSS), 6-9 Jan. 2014, Waikoloa, HI
 3. Goldis, E.A. ; Xiaoguang Li ; Caramanis, M.C. ; Keshavamurthy, B. ; Patel, M. ; Rudkevich, A.M. ; Ruiz, P.A., *Applicability of topology control algorithms (TCA) to a real-size power system*. 2013 51st Annual Allerton Conference on Communication, Control, and Computing (Allerton), 2-4 Oct. 2013, Monticello, IL
 4. P.A. Ruiz, A.M. Rudkevich, M.C. Caramanis, E.Goldis, E. Ntakou, *Reduced MIP Formulation for Transmission Topology Control*. Proc. of 50th Allerton Conf. Communication, Control Computing, Monticello, IL, Oct. 2012
 5. M.C. Caramanis, E. Goldis, P.A. Ruiz, A.M. Rudkevich *Power Market Reform in the Presence of Flexible Schedulable Distributed Loads. New Bid Rules, Equilibrium and Tractability Issues* Proc. of 50th Allerton Conf. Commun., Control Computing, Monticello, IL, Oct. 2012
 6. Michael C. Caramanis, Justin M. Foster, and Evgeniy Goldis, *Coupling of Day-Ahead and Real-Time Power Markets for Energy and Reserves Incorporating Local Distribution Network Costs and Congestion*, in Proc. of 48th Allerton Conf. Commun., Control Computing, Monticello, IL, pp. 42-49, Sep. 2010.

*Employment
History*

Newton Energy Group LLC, Cambridge, MA 2015 - Present Lead software architect on pCloud development using .NET for both the Microsoft and Amazon cloud environments. Consulting in the area of power system economics, operations, planning and market analysis. Development and application of algorithms and decision support tools for power market participants.

Charles River Associates, Boston, MA - Senior Associate, 2007-2011 Worked on modeling projects spanning market and transmission studies, asset valuations and financial contract modeling. Simulated the energy market in the US and Persian Gulf using GE MAPS. Worked on asset/contract evaluation projects, including both generation and transmission. Developed guidelines and methodology for modeling system reliability in Russia. Evaluated potential market power in the UK.

WebOracle, Atlanta, GA - Software Developer, 2006-2007

Developed applications in .NET. Implemented Data Warehouse solutions and Microsoft Analyses Services. Built several cubes and Data Mining Models. Developed business and data layers for reporting components (T-SQL)

Georgia Pacific, Atlanta, GA - Project Manager, 2005-2006

Worked on performance tuning VB.NET code. Estimated project timelines and cost, as well as developed project plans. Served as an internal business analyst and helped to finalize the application feature set. Worked with the internal SOX committee to ensure application security. Designed and developed portions of the application that used VB.NET and T-SQL.